nature methods

Brief Communication

https://doi.org/10.1038/s41592-023-01809-y

mScarlet3: a brilliant and fast-maturing red fluorescent protein

Received: 27 June 2022

Accepted: 27 January 2023

Published online: 27 March 2023

Check for updates

Theodorus W. J. Gadella Jr.[1] ✉, Laura van Weeren[1], Jente Stouthamer[1], Mark A. Hink[1], Anouk H. G. Wolters[2], Ben N. G. Giepmans[2], Sylvain Aumonier[3], Jérôme Dupuy[3] & Antoine Royant[3,4]

We report the evolution of mScarlet3, a cysteine-free monomeric red fluorescent protein with fast and complete maturation, as well as record brightness, quantum yield (75%) and fluorescence lifetime (4.0 ns). The mScarlet3 crystal structure reveals a barrel rigidified at one of its heads by a large hydrophobic patch of internal residues. mScarlet3 behaves well as a fusion tag, displays no apparent cytotoxicity and it surpasses existing red fluorescent proteins as a Förster resonance energy transfer acceptor and as a reporter in transient expression systems.

Red fluorescent proteins (RFPs) found in Anthozoa species[1] are structurally related to green fluorescent protein (GFP) found in *Aequoria victoria* and fold in highly similar yet tetrameric β-barrel structures[2]. Much effort has been devoted to monomerize RFPs. After the first, relatively dim, mRFP1 was described[3], other brighter variants were created as mCherry[4], TagRFP[5], mRuby3 (ref. [6]), mKate2 (ref. [7]) and FusionRed[8]; however, irrespective of improvements, all these second-generation RFPs still suffer from relatively low quantum yield, photochromicity or residual dimerization tendency. For this reason, we developed the mScarlet series of RFPs[9]. mScarlet displays the highest intrinsic brightness (multiplication of extinction coefficient and quantum yield), no photochromicity and is monomeric, but its maturation is relatively slow. mScarlet-I with lower intrinsic brightness is brighter in cells owing to faster and more complete maturation. Notably, in a recent study mCherry-XL with an equal fluorescence quantum yield (70%) as mScarlet was evolved, but owing to reduced maturation, the brightness in cells was half of mScarlet[10]. Obviously, a variant combining fast maturation and the highest possible intrinsic brightness is highly desirable. For instance, for building Förster resonance energy transfer (FRET) sensors with an RFP acceptor, the extent of RFP maturation defines the extent of donor quenching, whereas its intrinsic brightness determines the intensity of the sensitized emission, both contributing to high FRET contrast.

Because random mutagenesis to create brighter mScarlet variants proved unsuccessful[9], we devised a targeted approach toward amino acids surrounding Threonine-74, as this is the only mutated amino acid in mScarlet-I compared to mScarlet. With multiparameter screening[11], we evolved variants of mScarlet-I with a higher quantum yield and variants of mScarlet with faster maturation (Supplementary Note 1).

After several rounds of targeted and random mutagenesis we generated two final variants mScarlet3 and mScarlet-I3 (spectra are detailed in Fig. 1a,b). Spectroscopic evaluation of purified mScarlet3 (Extended Data Table 1) revealed that it has a quantum yield of 75%, and extinction coefficient of 104,000 M^{-1} cm^{-1} and it displays a long monoexponential fluorescence lifetime of 4.0 ns (Fig. 1c). Spectroscopic analysis of mScarlet-I3 revealed an enhanced quantum yield (65%) and an 21% increased intrinsic brightness compared to mScarlet-I, approaching that of mScarlet (95%) (Extended Data Table 1). Intrinsic brightness of purified fluorescent proteins (FPs), however, does not always report on the actual brightness found in cells, as the latter additionally depends on the extent and speed of chromophore maturation. Notably, in cells, mScarlet3 and mScarlet-I3 are 76% and 80% brighter compared to mScarlet and more than fivefold brighter than mCherry, owing to a substantially faster and more complete maturation (Extended Data Table 1, Fig. 1d and Extended Data Fig. 1). By directly comparing the intrinsic brightness with the cellular brightness, one can infer the overall extent of maturation. It was found that after 24 h, mScarlet3 matures to the same extent (96%) as the very efficiently maturing mScarlet-I (Fig. 1e). mScarlet-I3 maturation is more complete (113%) than mScarlet-I. mScarlet3 matures four times faster than mScarlet and equally as fast as mCherry (Extended Data Table 1 and Fig. 1f). mScarlet-I3 is the fastest maturing monomeric

[1]Section of Molecular Cytology and van Leeuwenhoek Centre for Advanced Microscopy, Swammerdam Institute for Life Sciences, University of Amsterdam, Amsterdam, the Netherlands. [2]Biomedical Sciences of Cells & Systems, University of Groningen UMC Groningen, Groningen, the Netherlands. [3]Université Grenoble Alpes, CNRS, CEA, Institut de Biologie Structurale, Grenoble, France. [4]European Synchrotron Radiation Facility, Grenoble, France. ✉e-mail: th.w.j.gadella@uva.nl

https://doi.org/10.1038/s41592-023-01809-y

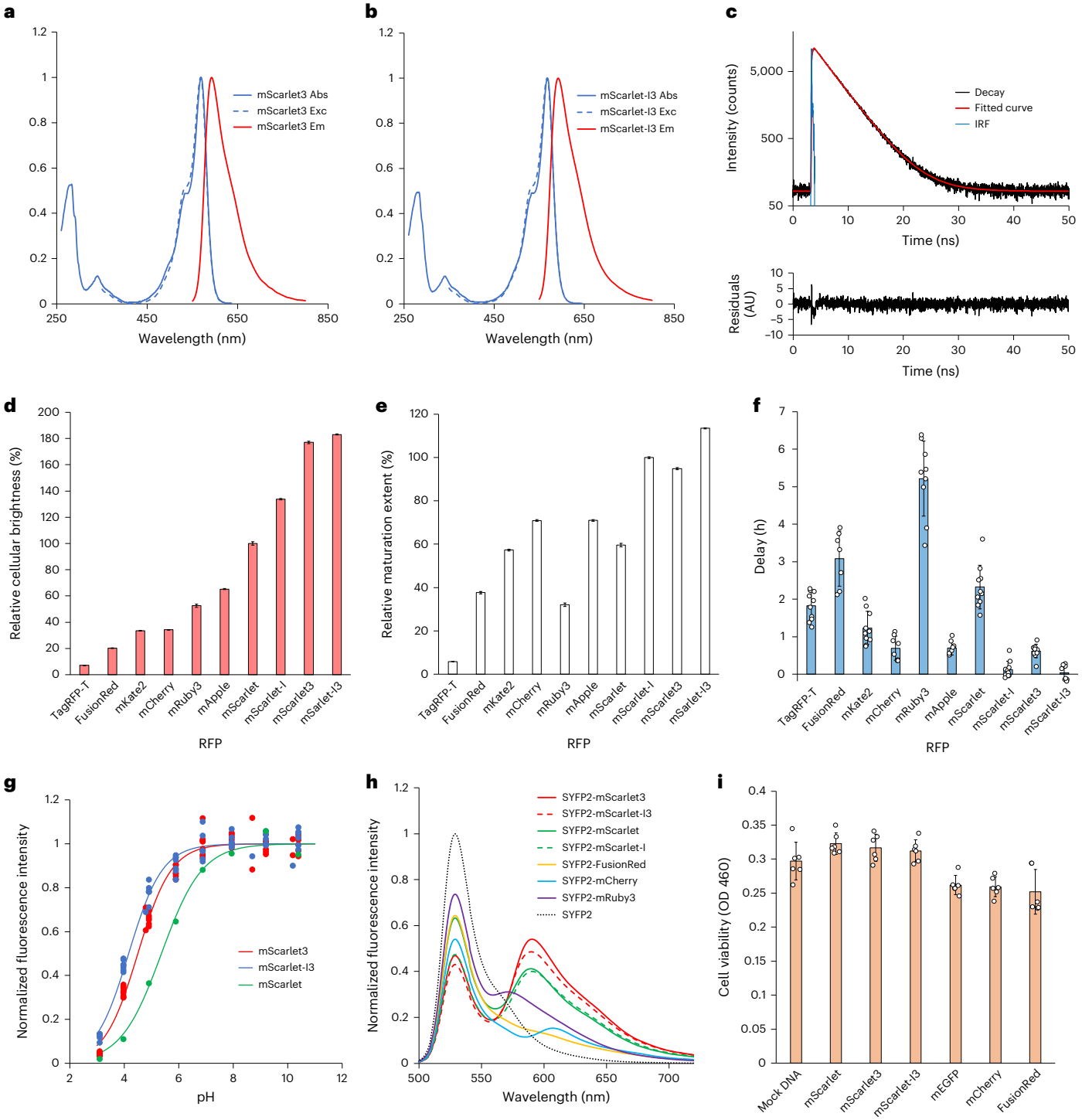

Fig. 1 | Characterization of mScarlet3 and mScarlet-I3. a,**b**, Normalized absorbance (Abs), excitation (Exc) and emission (Em) spectra of mScarlet3 (**a**) and mScarlet-I3 (**b**). For the fluorescence excitation spectra, the emission was set at 620 nm and for the fluorescence emission spectrum, excitation was set at 540 nm. **c**, Fluorescence decay of mScarlet3 (top) fitted with a single exponential lifetime of 3.96 ns. The weighted residuals (bottom) show a perfect fit ($\chi^2 = 1.18$). IRF, instrument response function; AU, arbitrary units. **d**, Relative brightness (mean ± s.d.) of RFPs in HeLa cells 24 h after transfection, determined by normalized, spectrally corrected ratios of red to cyan fluorescence intensity found in cells upon co-production of RFP and mTurquoise2 (Extended Data Fig. 1). **e**, Maturation extent of RFPs in HeLa cells relative to mScarlet-I (mean ± s.d.) 24 h after transfection calculated by dividing the cellular brightness (Fig. 1d) by the intrinsic brightness (Extended Data Table 1). **f**, Maturation speed of RFPs in mammalian cells measured as delay (mean ± s.d. in **h**) relative to co-produced mTurquoise2, $n = 7–10$ cells. **g**, pH dependence of the fluorescence intensity of mScarlet3, mScarlet-I3 and mScarlet. **h**, Spectral analysis of FRET between SYFP2 and diverse RFPs in living HeLa cells. All spectra are corrected for detector sensitivity and normalized to the unquenched SYFP2 signal. **i**, Check for cytotoxicity of fluorescent protein expression in HeLa cells 48 h after transfection quantified by NAD(P)H/live-cell-dependent conversion of WST-8 into blue-light-absorbing formazan (average absorbance at 460 nm ± s.d. for six independent transfections).

RFP tested. Of note, in alkaline denaturation experiments, we found a marked stability of mScarlet3: where mScarlet and mScarlet-I denature instantaneously (<1 s) at pH 13.5, mScarlet3 retained more than half of its initial fluorescence for over 40 min (Extended Data Fig. 2). mScarlet3 (pKa = 4.5) and mScarlet-I3 (pKa = 4.2) have better acid resistance compared to mScarlet(-I) (pKa = 5.4), which would be beneficial for applications of these RFPs in endomembrane studies (Fig. 1g and Supplementary Video 1). At high excitation power, the photobleaching kinetics are slightly faster compared to the precursors, with mScarlet3 performing better in confocal bleaching (Extended Data Table 1 and Extended Data Fig. 3a–d). Notwithstanding, mScarlet3 is photostable enough to permit 1,000 confocal scans under live-cell confocal timelapse imaging conditions without noticeable photobleaching (Supplementary Video 2). We also tested photochromicity in alternating blue and green excitation and we found that both mScarlet3 and mScarlet-I3 are non-photochromic (like mScarlet, mScarlet-I and mCherry; Extended Data Table 1 and Extended Data Fig. 3e), which is in contrast to mApple, mRuby3, TagRFP-T and FusionRed[9,12]. mKate2 and TagRFP-T showed increased red fluorescence after several photochromic cycles (Extended Data Fig. 3d,e). Photochromic behavior can be highly problematic in quantitative ratiometric FRET studies[9]. mScarlet3 and mScarlet-I3 display monoexponential fluorescence decay with long lifetimes of 4.0 and 3.6 ns, respectively, facilitating possible application as donors in FRET with fluorescence lifetime imaging (FLIM).

As both mScarlet3 and mScarlet-I3 contain new N and C termini and various mutations on the exterior of the β-barrel (Supplementary Note 1 and Supplementary Fig. 1), we performed an OSER (organized smooth ER) assay to address their monomeric behavior[13]. Indeed, the OSER test revealed no enhanced oligomerization (Extended Data Table 1 and Extended Data Fig. 4a–h).

Several fusion constructs with mScarlet3 to label specific cellular organelles and structures were made. In all instances bright labeling of the correct structures and localizations was found (Fig. 2a–f, Extended Data Fig. 4i–l and Supplementary Video 3). Also, the direct fusion to α-tubulin, which is known to be very adversely affected by residual dimerization tendency of FPs, revealed distinct microtubular structures displaying dynamic instability[14] (Supplementary Video 4).

The new mScarlets are superior FRET acceptors of a monomeric yellow fluorescent protein (YFP) SYFP2: in ratiometric spectral FRET, mScarlet3 quenches SYFP2 fluorescence intensity as efficiently as mScarlet-I (both 53%) and better than mCherry (46%) or mScarlet (37%) (Fig. 1h and Extended Data Fig. 5a,b). The yield in sensitized emission is substantially improved for mScarlet3 (140% compared to mScarlet-I, 154% compared to mScarlet and 377% compared to mCherry). The better quenching of SYFP2 is also seen by FLIM analysis of the τ_φ fluorescence lifetime of SYFP2, which is more reduced with mScarlet3 (1.67 ns) than with mScarlet (1.85 ns) or mCherry (1.77 ns) (Extended Data Fig. 5c). We found a small negative effect of the new N and C termini on FRET levels, possibly due to another average orientation despite our efforts in keeping the linker length identical in the comparison of the diverse fusions (Extended Data Table 1 and Extended Data Fig. 5). Although mScarlet-I3 is a slightly better quencher of SYFP2 than mScarlet3, it produces less sensitized emission due to its lower quantum yield. Hence, mScarlet3 is the best FRET acceptor of YFPs, providing equal YFP quenching but 40% more sensitized red emission compared to mScarlet-I (the previously best-performing RFP).

Because mScarlet3 and mScarlet-I3 incorporate C and N termini originally described for mScarlet-I2 (ref. [15]), for which it was shown to reduce cytotoxicity in bacteria, we tested for cytotoxicity in mammalian cells. Within 48 h after transfection, we found no apparent cytotoxicity of mScarlet3 or mScarlet-I3 expression (Fig. 1i). By monitoring fluorescently labeled cells at 4 and 6 d after transfection, we found slightly more cells producing mScarlet-I3 or mScarlet3 compared to other RFPs (Extended Data Fig. 6), also suggesting no apparent cytotoxicity. We tested the resistance to paraformaldehyde fixation, where mScarlet3 proved to be the brightest RFP variant after fixation (Extended Data Fig. 7).

To understand the structural basis for the improvements found in mScarlet3, we determined its crystal structure at physiological pH at 1.33 Å resolution (Methods and Supplementary Note 2). The conformations of the chromophore and its surrounding residues (first coordination sphere) are perfectly superimposable on those observed in the pH 7.8 crystal structure of mScarlet[9]. Yet, the key residue Glu216 adopts two alternate conformations, such as in the bright green FP, enhanced GFP (eGFP) (Fig. 2g). We focused our analysis on the mutations within the bulk of the protein barrel: Y84W, Y194F, V196I and G220A. Coincidentally, these four mutations remove two polar atoms and add six non-polar atoms, which results in the replacement of a small amphipathic cavity by a hydrophobic patch purely involving methyl or methine carbon atoms (Fig. 2h). This hydrophobic patch is linking together the tips of 4 of the 11 β-strands of the protein and of the chromophore-bearing α-helix, as well as a loop and a helix bridging pairs of strands (Extended Data Fig. 8). Thereby it contributes to the increased rigidification of one head of the β-barrel and the increased fluorescence QY of mScarlet3.

To assess the performance of mScarlet3 for in vivo applications, we first compared mScarlet and mScarlet3 for brightness in zebrafish larvae. At 24 h after injection of plasmid, a twofold increase in red fluorescence was detected in mScarlet3 in larvae (Fig. 2i), in good agreement with the values found in mammalian cells (Fig. 1d and Extended Data Figs. 1 and 7). Additionally, injections were performed of H2B-mScarlet3 produced in exocrine cells of the pancreas (Fig. 2j and Supplementary Video 5). Finally, we imaged H2B-mScarlet3 for 6 h in 5-min intervals (z-stack of 309 frames) in all cells in zebrafish larvae following messenger RNA injection and found many cells going through mitosis (Fig. 2k and Supplementary Videos 6 and 7). Thus, mScarlet3 is useful for in vivo examination of cells in zebrafish larvae.

Fig. 2 | Characterization of the cellular and in vivo applications of mScarlet3 and of the mScarlet crystal structure. a–**f**, Usage of mScarlet3 as a fusion tag in HeLa cells. Scale bar, 10 µm. Red fluorescence intensity was scaled according to the mScarlet LUT (**a**) micrographs that are representative of at least four images in two independent transfections. Cells were producing ER-mScarlet3 (**a**, endoplasmic reticulum); LaminB-mScarlet3 (**b**, nuclear envelope); 4xmito-mScarlet3 (**c**, mitochondria); lifeact-mScarlet3 (**d**, actin cytoskeleton); mScarlet3-peroxi (**e**, peroxisomes); and LCK-mScarlet3 (**f**, plasma membrane). **g**, Alternate conformations of Glu216 in mScarlet3. $2F_{obs} - F_{calc}$ electron density map contoured at a 1.5-σ level and superimposed on the chromophore and the surrounding residues. Glu216 unambiguously exhibits two distinct conformations of its side chain, leading to the positioning of one water molecule in alternate conformations. **h**, Comparison of a region near one head of the β-barrel between mScarlet (blue) and mScarlet3 (magenta), showing how the concerted mutations of four residues lead to the formation of a hydrophobic patch. Arrows indicate the additional non-polar atoms introduced in mScarlet3 contributing to both the volume decrease of a small amphipathic cavity and the increase in the number of potential van der Waals interactions. **i**, Brightness of mScarlet (green symbols) and mScarlet3 (red symbols) in fixed zebrafish larvae 24 h after injection. Points represent measurements of average fluorescence intensity found in confocal pictures of individual cells relative to a co-produced mTurquoise2; lines represent linear regression through the origin. CFP, cyan fluorescent protein. **j**, mScarlet3 applied for live-cell imaging of pancreatic cells in zebrafish. H2B-mScarlet3 was expressed under an elastase promotor and examined on a lightsheet microscope. Nuclear localization is found in the exocrine cells of the pancreas. Note the cell division in the boxed area. Scale bar, 5 µm. **k**, Lightsheet microscopy of H2B-mScarlet3-labeled cell nuclei in a developing zebrafish larva (see also corresponding Supplementary Video 6). Scale bar, 100 µm.

https://doi.org/10.1038/s41592-023-01809-y

In conclusion, we have evolved a new RFP mScarlet3, which combines the highest quantum yield of RFPs, monomeric behavior, no apparent cytotoxicity and absence of photochromic behavior with fast and complete maturation (Extended Data Fig. 9). In all tested fusions, mScarlet3 demonstrated excellent performance as a fusion tag, a FRET acceptor and in live-cell applications. While chromophore rigidity is essential for high quantum yield, too much rigidity may hamper FP maturation, which requires a certain degree of internal flexibility to assist fast kinetics of chromophore formation and oxidation. We speculate that the engineered hydrophobic patch (Fig. 2h) performs that function. We do not exclude that other existing bright FPs can be still improved to combine maximal brightness and maturation by following the same recipe of multiparameter (at least brightness and fluorescence lifetime) screening[11].

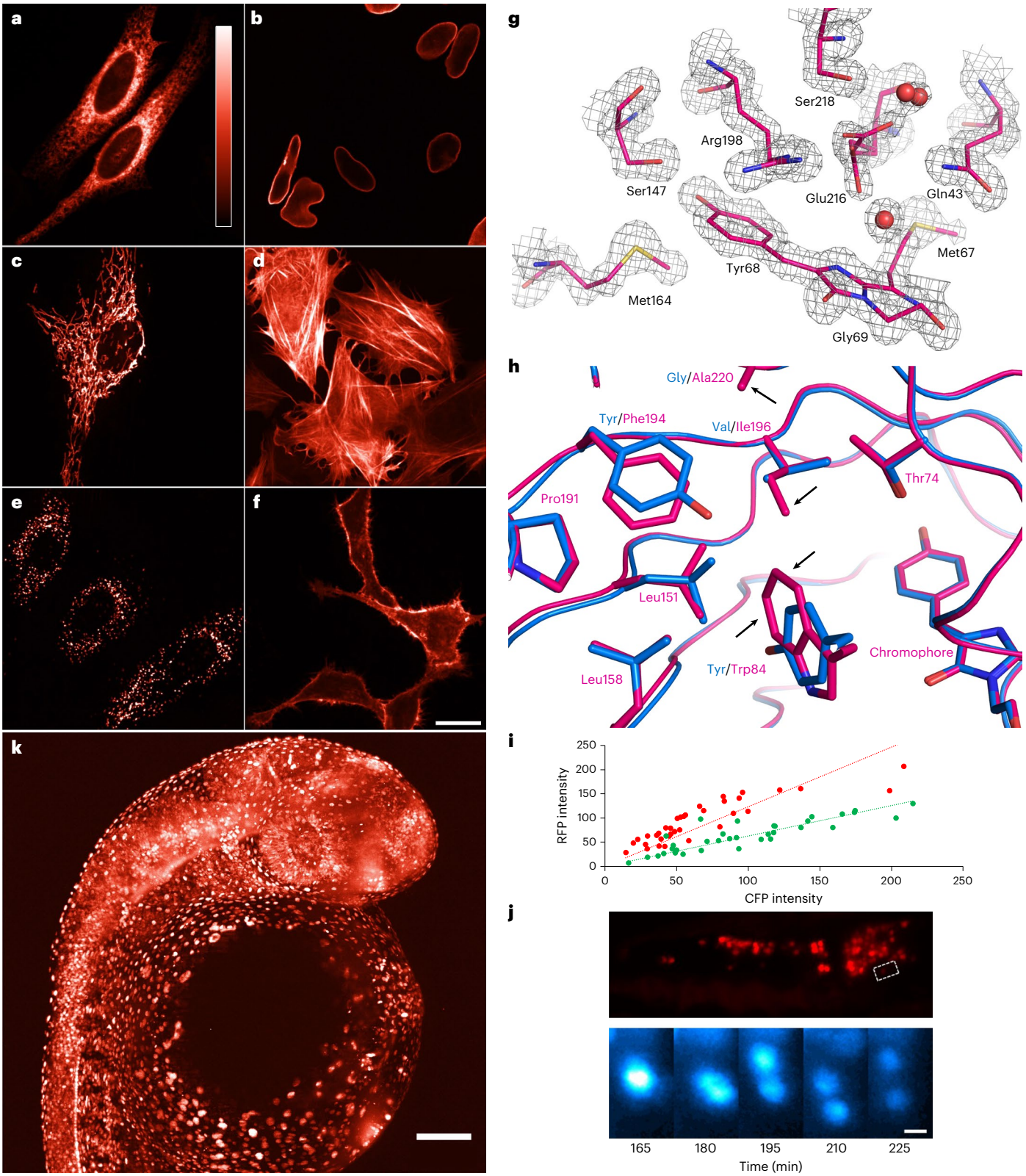

Online content

Any methods, additional references, Nature Portfolio reporting summaries, source data, extended data, supplementary information, acknowledgements, peer review information; details of author contributions and competing interests; and statements of data and code availability are available at https://doi.org/10.1038/s41592-023-01809-y.

References

1. Matz, M. V. et al. Fluorescent proteins from nonbioluminescent Anthozoa species. *Nat. Biotechnol.* **17**, 969–973 (1999).
2. Yarbrough, D., Wachter, R. M., Kallio, K., Matz, M. V. & Remington, S. J. Refined crystal structure of DsRed, a red fluorescent protein from coral, at 2.0-Å resolution. *Proc. Natl Acad. Sci. USA* **98**, 462–467 (2001).
3. Campbell, R. E. et al. A monomeric red fluorescent protein. *Proc. Natl Acad. Sci. USA* **99**, 7877–7882 (2002).
4. Shaner, N. C. et al. Improved monomeric red, orange and yellow fluorescent proteins derived from *Discosoma* sp. red fluorescent protein. *Nat. Biotechnol.* **22**, 1567–1572 (2004).
5. Merzlyak, E. M. et al. Bright monomeric red fluorescent protein with an extended fluorescence lifetime. *Nat. Methods* **4**, 555–557 (2007).
6. Bajar, B. T. et al. Improving brightness and photostability of green and red fluorescent proteins for live cell imaging and FRET reporting. *Sci. Rep.* **6**, 20889 (2016).
7. Shcherbo, D. et al. Far-red fluorescent tags for protein imaging in living tissues. *Biochem. J.* **418**, 567–574 (2009).
8. Shemiakina, I. I. et al. A monomeric red fluorescent protein with low cytotoxicity. *Nat. Commun.* **3**, 1204 (2012).
9. Bindels, D. S. et al. mScarlet: a bright monomeric red fluorescent protein for cellular imaging. *Nat. Methods* **14**, 53–56 (2017).
10. Mukherjee, S. et al. Directed evolution of a bright variant of mCherry: suppression of nonradiative decay by fluorescence lifetime selections. *J. Phys. Chem. B* **126**, 4659–4668 (2022).
11. Bindels, D. S., Postma, M., Haarbosch, L., van Weeren, L. & Gadella, T. W. J. Multiparameter screening method for developing optimized red-fluorescent proteins. *Nat. Protoc.* **15**, 450–478 (2020).
12. Shaner, N. C. et al. Improving the photostability of bright monomeric orange and red fluorescent proteins. *Nat. Methods* **5**, 545–551 (2008).
13. Costantini, L. M., Fossati, M., Francolini, M. & Snapp, E. L. Assessing the tendency of fluorescent proteins to oligomerize under physiologic conditions. *Traffic* **13**, 643–649 (2012).
14. Costantini, L. M. et al. A palette of fluorescent proteins optimized for diverse cellular environments. *Nat. Commun.* **6**, 1–13 (2015).
15. Valbuena, F. M. et al. A photostable monomeric superfolder green fluorescent protein. *Traffic* **21**, 534–544 (2020).

Methods

General methods

All RFPs were cloned into a pDRESS plasmid (Addgene 130509)[11] or pDX vector (a modified TriEX vector, expressing an FP in both bacteria, under a rhamnose promoter, and in mammalian cells, under a CMV promoter) using the AgeI and BsrGI restriction sites. mRuby3 (ref. [6]), TagRFP-T[12], mApple[12], mCherry[4] mKate2 (ref. [7]) and FusionRed[8] were obtained as described previously[9]. The new vectors pDRESS_mTurquoise2_spatial-linker-P2A_mScarlet3 (189752, Addgene), pDx_mScarlet3 (189754, Addgene), pDRESS_mTurquoise2_spatial-linker-P2A_mScarlet-I3 (189755, Addgene), pDx_mScarlet-I3 (189757, Addgene) were deposited at Addgene. Mammalian cell imaging was conducted with U2OS cells (HTB-96, ATCC) or HeLa cells (CCL-2 ATCC). Mammalian cells were grown in glass-bottomed 24-well plates (MatTek P24G-1.5-13-F) in DMEM (61965059, Thermo Fisher Scientific) containing 10% fetal bovine serum (10270106, Thermo Fisher Scientific) or with colorless DMEM (11594416, Thermo Fisher Scientific) supplemented with 1% Glutamax (11574466, Thermo Fisher Scientific) under 7% humidified CO_2 atmosphere at 37 °C. For transfection polyethyleneimine (PEI) in ddH_2O (1 mg ml^{-1}, pH 7.3; 23966, Polysciences) was used. The transfection mixture was prepared in Opti-MEM (31985047, Thermo Fisher Scientific) with 2 µl PEI solution and 50–200 ng plasmid. For some transfections, carrier DNA (empty plasmid) was added to prevent overexpression. The transfection mixture was incubated for 20–45 min. Cells were used for imaging 15–48 h after transfection.

Mutagenesis

mScarlet variants were obtained by site-directed and random mutagenesis using standard protocols[9]. Evolution started from mScarlet and mScarlet-I by introducing G220A (Seq-IDs 3 and 4; Supplementary Fig. 1), followed by V196I (Seq-IDs 5 and 6) targeted mutagenesis. With random mutagenesis, the combination of T107S, G156V and E219V was found to be beneficial. A new template mScarlet-2A (Seq-ID 7) was ordered as geneblock carrying T107S, G156V, V196I, E219V and G220A as mutations relative to mScarlet. T74I was introduced into mScarlet-2A to yield mScarlet-2A-I (Seq-ID 8). Y84W was introduced in mScarlet-2A by targeted mutagenesis, yielding mScarlet-2A-84W (Seq-ID 9). We also introduced T74I into mScarlet-2A-84W to yield mScarlet-I-2A-84W (Seq-ID 10). These two new templates were subjected to an additional round of random mutagenesis. From screening of several variants of mScarlet-2A-84W were found with increased maturation, one with two mutations T109A, K183R, one with the single mutation Y194F and one with the single mutation K48R with increased brightness. We first combined T109A, K183R and Y194F, yielding mScarlet-2A-84W-R8-194F (Seq-ID 11). Introducing K48R yielded a slight further brightness increase in mScarlet3-NCwt (Seq-ID 13). With PCR different N and C termini[15] were introduced (Δ1, V2M, S3D, K4S, G5T and M227S, D228G, E229G, S230S, Δ231 and Δ232) yielding mScarlet3 (Seq-ID 15). In the random mutagenesis of mScarlet-2A-I-84W a combination of six mutations originating from different mutated variants were found to be beneficial. These mutations were introduced by ordering a new template mScarlet-I-2A-84W-nt1 (Seq-ID 12) containing K93R, N99I, A105T, T128G, K140R and Y194F relative to the mScarlet-2A-I-84W template. Subsequent scrutinizing demonstrated that reversal of R93K by targeted mutagenesis was beneficial yielding mScarlet-I3-NCwt (Seq-ID 14). With PCR, new N and C termini were introduced (Δ1, V2M, S3D, K4S, G5T and M227S, D228G, E229G, S230S, Δ231 and Δ232) yielding mScarlet-I3 (Seq-ID 16).

Protein purification

His-tagged recombinant RFPs were purified from *Escherichia coli* bacteria as described[9] except for the final affinity purification and dialysis steps. For affinity purification the crude *E. coli* protein extract was obtained from defrosted *E. coli* pellets and incubation on ice with 5 ml ST buffer (20 mM Tris-HCl and 200 mM NaCl, pH 8.0) supplemented with lysozyme (1 mg ml^{-1}, L7651, Sigma-Aldrich), benzoase nuclease (5 U ml^{-1}, Merck/Millipore, 71205-3) and 50 µl 100× Halt Protease Inhibitor Cocktail (Thermo Scientific, 87785). After 2 h of incubation, 100 µl of 10% (v/v) NP-40 (Thermo Fisher Scientific, 85124) was added to the lysate, after which it was centrifuged (30 min, 40,000*g* at 4 °C). The supernatant was added to 2 ml of Co^{2+}-loaded HisPurTM Cobalt Superflow Agarose resin (Thermo Scientific, 25228) and incubated for at least 1 h at 4 °C. The resin was washed 9–10 times with 2 ml wash buffer (ST buffer supplemented with 15 mM imidazole) until no detectable protein (as measured by OD at 280 nm) was washed from the resin. His-tagged proteins were eluted with 2 × 1 ml elution buffer (ST buffer supplemented with 150 mM imidazole). The eluent was desalted and obtained in a 10 mM Tris-HCl, pH 8.0, solution using Sephadex-G25 desalting columns (GE Healthcare 17-0852-01). Proteins were short-term stored at 4 °C or flash-frozen and stored at −80 °C for long-term storage.

Spectroscopy

Extinction coefficient. Purified proteins were diluted in PBS (50 mM Na_2HPO_4–NaH_2PO_4, 137 mM NaCl and 2.7 mM KCl, pH 7.4). Absorbance spectra were acquired with a spectrophotometer (Libra S70, Biochrom). The spectra were recorded in the wavelength range of 260–700 nm, with a step size of 1 nm. PBS was used as a background reference. The samples were diluted such that the absorbance of the red chromophore peaked between 0.15 and 0.5. To denature the RFPs 10–200 µl 10 M NaOH was subsequently added to the samples, which was directly mixed by pipetting. Spectra were acquired continuously after addition of the sodium hydroxide until the absorbance spectra showed a complete loss of the absorbance peak associated with the red chromophore and displayed only the peak associated with the green chromophore at 457 nm. This absorbance spectrum was used for further analysis and, if necessary, the average absorbance value in the wavelength range 670–680 nm was subtracted from the spectra to correct for a minor offset. The concentration of the denatured green chromophore was calculated assuming an extinction coefficient of 44,000 M^{-1} cm^{-1} at 457 nm for the green chromophore in the denatured RFP[16,17]. Based on the concentration of the red chromophore, the extinction coefficient for the red chromophore was determined at the maximum absorbance wavelength. The above procedure was repeated at least three times per RFP variant and the average extinction coefficient was calculated.

Quantum yield. Purified proteins were diluted in PBS (50 mM Na_2HPO_4–NaH_2PO_4, 137 mM NaCl and 2.7 mM KCl, pH 7.4). Absorbance spectra were recorded with a spectrophotometer (Libra S70, Biochrom) in the wavelength range 260–700 nm with a step size of 1 nm. PBS was used as a background reference. Three dilutions of each RFP variant were prepared with an absorbance at 540 nm (A_{540}) of $0.005 < A_{540} < 0.05$. Fluorescence emission spectra were taken from the same sample cuvette with a fluorimeter (Model FP-8500, Jasco with a red extended PMT tube model R928-23, operated by Jasco Spectral Manager v.2.15). The excitation wavelength was set at 540 nm, the emission spectrum was recorded from 550–800 nm with a step size of 1 nm at a scan speed of 200 nm min^{-1}. The excitation as well as the emission slits were set at 2.5 nm. To obtain more accurate A_{540} absorbance values of the low absorbing samples, their absorbance spectra were fitted to an absorbance spectrum of the same RFP at high concentration (optical density (OD) 0.1–0.3) and a variable (constant) offset value using a linear least squares fit. The A_{540} absorbance of the quantum yield samples was obtained from the fitted spectral component. Fluorescence spectra were background corrected by subtracting a spectrum measured with PBS. The emission spectra were corrected for spectral sensitivity using a calibrated white light source (ESC-842, Jasco) and the spectral area (I_{em}) was obtained by integrating from 550–800 nm. The absorbance at 540 nm (A_{540}) was plotted versus the area under the emission spectrum, subsequently the slope of the line was determined using linear

regression. The regression lines were constrained to go through the origin, hence $I_{em} = a \times A_{540}$.

Equation 1 was used to calculate the quantum yield:

$$QY_s = QY_r \frac{a_s}{a_r} \quad (1)$$

In Equation 1, QY denotes the quantum yield (*s* and *r* denote sample and reference RFP, respectively) and *a* corresponds to the acquired slope. mScarlet was used as a reference with a quantum yield of 0.704 (ref. [9]).

Fluorescence lifetime. Fluorescence lifetime measurements of purified RFPs diluted in PBS (50 mM Na_2HPO_4–NaH_2PO_4, 137 mM NaCl and 2.7 mM KCl, pH 7.4) were performed at an Olympus FV1000 confocal microscope equipped with a PicoHarp 300 TCSPC module (PicoQuant operated with SymPhoTime v.64.2.1) as described[9].

pH dependence of RFP fluorescence intensity. A pH buffer series was created (pH 3–10) using a universal 50 mM citric acid, 50 mM phosphoric acid, 50 mM boric acid and 100 mM NaCl buffer. Buffers at the desired pH were made by titrating a 2× concentrated stock solution with 1 M NaOH (Merck 109137) and adjusting the volume to obtain a two-fold dilution. Citric acid and phosphoric acid (85%) were from Merck (818707 and 563, respectively), boric acid was from Sigma (B-0252). The final pH value was measured 24 h after preparation at room temperature and yielded pH values of 2.96, 3.90, 4.85, 5.94, 6.89, 8.16, 9.21 and 10.75. Purified RFPs (see 'Purification' section) were diluted in a black µ-clear 96-well plate (655090, Greiner). For each pH, triplicate samples for one RFP were made ranging from pH 3.0–10.8. With a Biotek FL-600 fluorescence plate reader using the KC4 v.3.0 software, the fluorescence intensity was measured using a 555/25 excitation filter and a 620/40 emission filter. The curves of pH versus fluorescence of the samples, *F*(pH), was fitted using the Hill-function, Equation 2, to obtain the apparent pKa of the RFP and the Hill coefficient *n*:

$$F(\mathrm{pH}) = \frac{F_{max}}{1 + 10^{n(\mathrm{pKa}-\mathrm{pH})}} \quad (2)$$

For Fig. 1g data from three technical replicates were pooled into one dataset for mScarlet3 and mScarlet-I3.

Stability at pH 13.5. Fluorescence intensity was monitored as a function of time in a fluorimeter (Model FP-8500, Jasco with a red extended PMT tube model R928-23) using 560 nm excitation and 610 nm emission (slits at 5 nm). Measurements were started with blank PBS solution (50 mM Na_2HPO_4–NaH_2PO_4, 137 mM NaCl and 2.7 mM KCl, pH 7.4) to which 10 µl of purified RFP was added. After 1 min 100 µl of 2 M NaOH was added and the mixture was quickly mixed by pipetting up and down in the cuvette. To determine the stability of RFP fluorescence at alkaline pH, the blank intensity was subtracted and the signal was normalized to the blank-corrected RFP fluorescence signal at normal pH. The signal after addition of NaOH was corrected for dilution. After NaOH addition the final unbuffered NaOH concentration was 0.33 M, yielding a pH of 13.5. Stability measurements were performed in duplicate yielding essentially similar results.

Cellular microscopy-based methods

Brightness in mammalian cells. The brightness of the diverse RFPs was determined in U2Os and HeLa cells as described previously[11]. Briefly, 50 ng of pDress vector encoding a 1:1 expression of mTurquoise2 CFP and the respective RFP was mixed with 150 ng carrier DNA and transfected in mammalian cells in glass-bottomed 24-well plates as described under the general methods section. At 24 h after transfection cyan, yellow and red fluorescence images were recorded on a Nikon widefield microscope. The widefield microscope consisted of an Eclipse Ti-E (Nikon) equipped with 440, 508 and 555 nm LEDs (SpectraX, Lumencor). The excitation light from these LEDs was passed through a 440/20, 510/24 or 550/15 nm bandpasses, respectively. For 440 nm and 508 nm excitation, a triple-band cube (MXU74157, Nikon) was used, for 555 nm excitation a quad band cube (MXU 71640, Nikon) was used. Emission was additionally filtered with a 479/40, 550/49 nm or 593/46 nm bandpasses (all from Semrock) placed in an optical filter changer (Lambda 10-B, Sutter instrument). For the three detected channels cyan, yellow and red, the effective excitation and emission bands were cyan, 430–450 nm excitation and 459–490 nm emission; yellow, 498–523 nm excitation and 526–555 nm emission; and red, 543–558 nm excitation and 570–616 nm emission. A ×10 CFI Plan Apochromat NA 0.45 (Nikon MRD00105) objective was used. Images were acquired on an ORCA-Flash4.0 v.2 Digital CMOS camera (C11440-22CU, Hamamatsu Photonics) using Nikon NIS Elements AR v.4.51.01 64 bit. For each well a 5 × 5 tile of images of 512 × 511 pixels each was acquired using a central region of interest (ROI) of 1,024 × 1,022 pixels with 2 × 2 binning and automated image stitching with 10% overlap, resulting in a final image size of 2,253 × 2,253 pixels corresponding to a 2.91 × 2.91 mm imaged area in each well. LED power was 10 %, 20% and 10% for 440, 508 and 555 nm LEDs for the cyan, yellow and red images, respectively. Integration time per image was 60 ms, 200 ms and 60 ms for the cyan, yellow and red images, respectively. The ratio of red to cyan fluorescence was calculated using the ratio_96-wells_macro_v.7 as described[11]. The brightness in mammalian cells was obtained by correcting these ratios for spectral throughput of the imaging device. To this end, spectra of the corresponding purified RFPs were used and the average excitation in the 543–558 nm excitation bandpass was calculated from the normalized excitation spectrum and the integrated fluorescence in the 570–616 bandpass was divided by the total integrated emission (550–800 nm). These corrections were normalized to the throughput for mScarlet. Consequently, the detected red/cyan ratios were multiplied by 1.0 for mScarlet, 1.015 for mScarlet-I, 0.985 for mScarlet3, 0.964 for mScarlet-I3, 1.522 for mCherry, 0.919 for mApple, 0.667 for TagRFP-T, 0.696 for mRuby3, 1.245 for FusionRed and 3.066 for mKate2 to obtain the relative cellular brightness values corrected for spectral throughput. Cellular brightness experiments were repeated at least five times in different months and in different cell types and yielded essentially similar results.

Brightness in mammalian cells after fixation. The brightness of the diverse RFPs was also determined after paraformaldehyde fixation in HeLa cells. Transfection, imaging and quantification was performed as described above for living cells, but before determining the red to cyan fluorescence ratio, cells were washed once with PBS and subsequently fixed for 20 min at room temperature with freshly prepared 4% paraformaldehyde in PBS. After fixation, cells were washed once with PBS and taken up in microscopy medium (140 mM NaCl, 5 mM KCl, 1 mM $MgCl_2$, 1 mM $CaCl_2$, 10 mM glucose and 20 mM HEPES, pH 7.4) and imaged on the same day.

Maturation. The extent of maturation was calculated by dividing the corrected cellular brightness by the intrinsic brightness (Extended Data Table 1) for the respective RFP and normalizing to mScarlet-I.

For measuring the maturation speed, the same cells, transfection and setup as described for the brightness in mammalian cells was used. For image acquisition the yellow image was omitted and the cyan and red single image using the full sensor ROI at 2 × 2 binning was used. Starting 5 h after transfection, for each well in the 24-well plate a red and cyan image was recorded every 15 min for 24 h. ROIs were manually drawn around 6–12 individual cells in each timelapse that remained viable for prolonged time and showed steady FP accumulation over time, but that started with no visible FP accumulation. The background corrected average intensity in the ROI was calculated for both the

cyan and red channels. Subsequently, only traces that first showed a nonlinear increasing accumulation of both RFP and CFP fluorescence, followed by a linear increasing accumulation and ending with a slowing down of the increase were selected. Cells with discontinuous time traces (due to cell division or apoptosis) were discarded. The RFP and CFP trace were normalized to maximal intensity and a straight line was fitted to the curve at the point a maximal slope of normalized fluorescence increase with time was calculated. The intercept of this line with the time axis was calculated and the delay between the intercept found for the red and cyan curves were calculated for 6–15 individual cell traces and averaged.

FRET-FLIM. For all RFPs, direct fusion constructs with SYFP2 were generated using PCR and restriction-enzyme-based cloning. To enable a good comparison, the linker between the SYFP2 and RFP was chosen such that a constant number of amino acids separated the two β-barrels in the fusion construct (correcting for differences in the length of N and C termini). In Supplementary Table 1, the linker sequence between the different RFPs and SYFP2 is described for the constructs used for the FRET studies depicted in Fig. 1h and Extended Data Fig. 5.

Then 50 ng of the SYFP2–RFP fusion constructs, SYFP2 or RFP single FP constructs, together with 150 ng of carrier DNA were transfected in HeLa cells growing in glass-bottomed 24-well plates as described above. At 46 h after transfection, the samples were analyzed with FRET-FLIM with a frequency domain widefield FLIM setup as described[11]. Briefly, the setup consisted of a Nikon Ti-E inverted fluorescence microscope, with a Proscan-III automated stage, excitation filter wheel and a Lambert Instruments FLIM Attachment (LIFA) system including a multi-LED light source and a LI2CAM detector (Lambert Instruments) operated with LiFLIM v.1.2.23 . For measuring the SYFP2 lifetime a 506 nm LED modulated at 40 MHz was used (Lambert Instruments) and the excitation light was additionally filtered with a 500/24-nm excitation filter (BrightLine single-band bandpass filter; Semrock, cat. no. FF01-500/24). A filter cube with a 523-nm dichroic mirror (Semrock, cat. no. Di02-R514) and a 542/27-nm emission filter (BrightLine single-band bandpass filter; Semrock, cat. no. FF01-542/27-25) was used to separate excitation from the SYFP2 fluorescence emission. A ×40 CFI Plan Apochromat NA 0.95 air objective (Nikon) was used. For determining the phase and modulation of the modulated excitation light at the sample position, a diluted (OD < 0.05) Alexa488 (Thermo Fisher Scientific) solution in PBS was used, for which a monoexponential fluorescence lifetime of 4.03 ns was assumed. FLIM measurements were performed in culture medium at 37 °C under 5–7% CO_2 atmosphere. For each SYFP–RFP sample 3–4 FLIM stacks were acquired with a different field of view of approximately 20 cells each. The mean lifetime of all cells in each FLIM stack was determined and averaged for all stacks acquired from the same sample. Repeated experiments with independent transfections yield essentially similar results.

FRET-SPIM. At 48 h after transfection, the medium of the same samples as described under FRET-FLIM was replaced with microscopy medium (140 mM NaCl, 5 mM KCl, 1 mM $MgCl_2$, 1 mM $CaCl_2$, 10 mM glucose and 20 mM HEPES, pH 7.4) and spectral images were acquired at room temperature using a home-built spectral imaging setup as described[9,18]. Briefly the setup consisted of a Zeiss Axiovert 200 M fluorescence microscope, equipped with an HBO 100 Mercury lamp for excitation and an imaging spectrograph (Imspector v.7) coupled to a CCD camera (ORCA ER) operated using MATLAB 6.1 with the DCAMAPI interface. A ×10 plan Neofluar NA 0.3 objective was used. Two spectral images were recorded: one with a 500/20 nm excitation filter (Chroma Technology Incorporation), a 80/20 dichroic mirror (20/80bs, Chroma Technology Incorporation) and a LP530 nm emission filter (46-059, Edmund optics worldwide) to record the full spectra and one with a 577/20 nm excitation filter, (D577/20, Chroma Technology Incorporation), a 596 nm dichroic mirror (600dcxr, Chroma Technology Incorporation) and a 630/60 nm emission filter (HQ630/60, Chroma Technology Incorporation) to record the direct excited RFP acceptor signal. The spectra were extracted from the spectral images and analyzed as described[9]. Briefly, the direct excited acceptor spectrum was subtracted from the FRET spectrum by analyzing the spectra from single RFP transfected cells. Subsequently, the remaining donor and sensitized emission acceptor signals were obtained by spectral unmixing with linear least squares method using the unfused SYFP2 donor spectrum and unfused RFP acceptor spectrum as a reference. After spectral correction for detector sensitivity of the unmixed spectra, the amount of donor quenching (δ_{loss}) was calculated from the net sensitized emission (α) and the ratio of quantum yields of donor (Q_d) and acceptor (Q_a) according to $\delta_{loss} = \alpha Q_d/Q_a$. The spectral components δ_{loss} and α are expressed as number of photons, obtained by dividing the corrected unmixed sensitized emission spectrum by the unit area full emission acceptor reference spectrum. From the donor quenching (δ_{loss}) and the remaining detected donor (δ obtained by dividing the corrected unmixed remaining donor emission spectrum by the unit area full emission donor reference spectrum) the energy transfer efficiency E is calculated according to $E = \delta_{loss}/(\delta + \delta_{loss})$. Typically, 10–30 single cell spectra were analyzed per SYFP2–RFP fusion. The averaged spectra were normalized to the unquenched donor signal.

Localization. The giantin DNA coding sequence of FRB–ECFP(W66A)–giantin (67903, Addgene) was cloned in to pmScarlet3–C1, using the restriction enzymes BsrGI and BamHI. The following constructs pLifeAct–mTurquoise2 (36201, Addgene), pmTurquoise2–α-tubulin (36202, Addgene), pmTurquoise2–Peroxi (36203, Addgene), EB3-mTurquoise2 (98825, Addgene), LCK-mTurquoise2 (98822, Addgene) and ER-mTurquoise2 (36204, Addgene) were digested with AgeI and BsrGI to exchange mTurquoise2 for mScarlet3 yielding pLifeact-mScarlet3_N1 (189767, Addgene), pmScarlet3-α-tubulin_C1 (189768, Addgene), pmScarlet3-Peroxi_C1 (189769), pEB3-mScarlet3_N1 (189770, Addgene), pLCK-mScarlet3_C1 (189771, Addgene) and pER-mScarlet3_N1 (189772, Addgene), respectively. The 4xmts-mScarlet3 and 3xnls-mScarlet3 were created by digesting 4xmito-mNeongreen (Addgene 98875) and 3xnls-mNeongreen (Addgene 98875) with AgeI and BsrGI to exchange mNeongreen for mScarlet3, yielding p4xmts-mScarlet3_N1 (189774, Addgene) and p3xnls-mScarlet3_N1 (189775, Addgene). LaminB-mTurquoise2 (99830, Addgene) was digested with AgeI and BglII to exchange mTurquoise2 for mScarlet3 yielding pmScarlet3-LaminB_C1 (189776, Addgene).

HeLa cells (CCL-2, ATCC) were seeded in uncoated glass-bottomed 24-well plates (MatTek P24G-1.5-13-F) and transfected with 50 ng plasmid, 150 ng carrier DNA and 2 µg PEI. At 24 h after transfection, cells were imaged in culture medium at 37 °C and 5% CO_2 atmosphere using a spinning disk setup as described[9]. Briefly this microscope system consisted of a Nikon Eclipse Ti-E microscope equipped a 561 nm laser and a Yokogawa CSU X-1 spinning disk unit (operating at 5,000 r.p.m.). The excitation light was directed to the sample via a custom-made dichroic mirror 405/488/561/640 through a ×40 CFI Plan Apochromat NA 0.95 air objective (Nikon). The red fluorescence was filtered with a 585–675 nm bandpass (FF01-512/630-25 m, Semrock). Images were recorded with an iXon 897 EMCCD camera (Andor) controlled by Nikon NIS Elements AR v.4.51.01 64-bit. Images shown are representative of 3–4 images taken from at least two technical replicates.

Photostability. For widefield photobleaching experiment transfection, mounting conditions and the microscope used were identical to those described under the 'Brightness in mammalian cells' section. A ×20 Plan Fluor NA 0.5 air objective was used and a 555 nm LED was used and set at 100% power. A quad band cube (MXU 71640, Nikon) and 593/46 nm bandpass emission filter was used for detection. Cells were focused under weak CFP illumination conditions to prevent any RFP bleaching before the actual photostability measurement. A timelapse recording

was made under perfect focusing at continuous 555 nm excitation with 25 steps of 5 s each. A 1,024 × 1,024-pixel central ROI of the camera was used at 1 × 1 binning and 10 ms integration time. The power at the object plane was 3.96 W cm^{-2}.

For confocal photobleaching, the transfection and mounting conditions were identical as described under brightness in mammalian cells. The microscope, the microscope objective and filter settings were identical as described under localization. The 561 nm laser was operated at 100% power, resulting in an illumination power at the object plane of 6.14 W cm^{-2}. Cells were focused under weak CFP illumination conditions to prevent any RFP bleaching before the confocal bleaching. Under perfect focusing at continuous 561 excitation, ten images separated by 100 ms were recorded, followed by ten recordings separated by 400 ms, ten recordings separated by 2 s, ten recordings separated by 5 s, ten recordings separated by 10 s and ten recordings separated by 20 s, resulting in a final stack of 60 images each with an integration time of 50 ms.

Widefield photostability was analyzed using the Bleach_96wells_macro_v.9 macro as described[11]. On average, 5–15 cells per image were used for this automated analysis. For analysis of the confocal photostability, the average fluorescence of 3–6 individual cells in each recording was averaged and corrected for background fluorescence at each time point. The intensities were normalized to the intensity at t_0. For both confocal and widefield photostability measurements, the time axis was adjusted relative to (the uncorrected time axis of) mScarlet to account for differences in excitation efficacy and RFP quantum yield to mimic a situation where all RFPs start with emitting an equal number of photons s^{-1} per molecule at t_0 compared to mScarlet[12]. To estimate the time at which the FPs were bleached by 50%, a linear interpolation method was used between the two most adjacent time points. Repeated experiments (3–4 times) yield essentially similar results.

Prolonged confocal imaging. For evaluating photostability under live-cell confocal imaging conditions, pLifeact-mScarlet3_N1 (189767, Addgene) was transfected in HeLa cells glass-bottomed 24-well plates that were imaged 24 h later using a commercial Leica SP8 confocal microscope with 561 nm excitation (power at object plane 3 µW) using a ×63 NA 1.4 HC PL APO CS2 oil immersion objective operated with Leica LAS-X v.3.5.7.23325 64 bit. Fluorescence was recorded with a HyD detector using a detection bandpass of 575–650 nm. One thousand frames were recorded with two scans averaged per frame over a period of 16 h with a frame rate of one frame min^{-1} at a (single scan) pixel dwell time of 0.4 µs and pixel size of 0.18 × 0.18 µm.

Photochromicity. For photochromicity experiments, the transfection, mounting and microscope were identical as described for the widefield photostability measurements. RFPs were switched on with 100% 440 nm for 0.5 s (3.3 W cm^{-2} at the focal plane) and subsequently illuminated at 20% continuous 550 nm LED power (0.8 W cm^{-2} at the focal plane) for 15 s during which images were recorded every 300 ms. Five consecutive cycles of 440 nm on-switching and 15 s of continuous 550 illumination were executed, of which the 550 nm excited recordings were concatenated in a stack of 255 images in total for each RFP. Data were analyzed using the Bleach_96wells_macro_v.9 macro[11] to extract the average time traces. Each trace represents the average of 6–13 cells per RFP variant. Photochromicity (P) was calculated as described[9] from the RFP intensities just after 440 nm on-switching (I_a) and just before 440 nm on-switching (I_b) as $P = (I_a - I_b) / I_a$. The four values found for the five consecutive photochromicity cycles from the analysis of the average time traces per RFP were averaged and indicated ± s.d. in Extended Data Table 1.

Oligomerization analysis with OSER method. mScarlet-CytERM-N17, mScarlet-I-CytERM-N17, TagRFP-T-CytERM-N17 and mCherry-CytERM-N17 were cloned as described previously[9]. FusionRed-CytERM-N17, mScarlet3-CytERM-N17 (189778, Addgene), mScarlet-I3-CytERM-N17 (189777, Addgene) and mScarlet-I3-NCwt-CytERM-N17 (189779, Addgene) were cloned by digesting mCherry-CytERM-N17 with enzymes AgeI and BsrGI to cut out mCherry and replace it with the other RFPs. Cells were analyzed between 22 h and 24 h after transfection. Imaging was performed with the same microscope setup and transfection conditions as described under localization. To obtain an overview of many cells, 16 × 16 tile scans were acquired with 10% overlap and automated image stitching in NIS elements software leading to 7,040 × 7,040-pixel images corresponding to 1.4 × 1.4 mm imaged areas in each well. Cells were analyzed as described previously[13]. ROIs of representative cells were assembled for Extended Data Fig. 4. Two days after transfection, fast moving punctate structures become visible in addition to the reticulate ER structure, likely reflecting a degradation pathway involving the endolysosomal machinery. Using the same spinning disk microscope, timelapse imaging was performed at a frame interval of 0.32 s for Supplementary Video 1. Repeated experiments (at least $n = 2$) with independent transfections yielded essentially similar results.

Cytotoxicity. Cytotoxicity caused by expression of RFPs in cells was tested with a standard cell counting kit (96992, Sigma). This kit assesses living cells that produce NAD(P)H to convert WST-8 (2-(2-methoxy-4-nitrophenyl)-3-(4-nitrophenyl)-5-(2,4-disulfophenyl)-2H tetrazolium, monosodium salt) into formazan, which can be detected by its blue light absorbance[19]. We used standard conditions for inducing expression of FPs by PEI-mediated transient transfection of HeLa cells in a 96-well format[11,20]. On day 0, 3,000 HeLa cells were seeded per well in 100 µl DMEM in a Greiner (cat. no. 655180) 96-well plate that was subsequently placed in a 37 °C humidified incubator with 5% (v/v) CO_2. On day 1, 300 ng mEGFP-pDx, pmScarlet-pDx, pmScarlet3-pDx (189754, Addgene), pmScarlet-I3-pDx (189756, Addgene), pmCherry-pDx or pmFusionRed-pDx was transfected with 1 µl 1‰ (w/v) PEI and 19 µl optimum mix, which was added per well in the 96-well plate. As a control, 300 ng empty pDx vector (carrier DNA) without an open reading frame was transfected. As a blank, we used wells without HeLa cells that contained only 100 µl DMEM. After transfection, the 96-well plate was returned to the humidified cell incubator. Under these conditions about 50–70% of the cells are transfected. On day 3, 48 h after transfection, 50 µl from a mix of 5.5 ml (containing 1 ml WST-8 cell counting kit, (96992, Sigma) and 4.5 ml DMEM), was added to each well followed by 2 h incubation at 37 °C and 5% CO_2. Then the absorbance at 460 nm was recorded using a Biotek FL-600 fluorescence/absorbance plate reader equipped with a 460/40 absorbance filter operated with BioTek KC4 v.3.0. The average absorbance (± s.d.) of six wells that were transfected with the same plasmid was determined and corrected for blank to quantify possible cytotoxicity. The experiment shown in Fig. 1i was replicated three times and once in U2Os cells with similar results.

Cell viability. On day 0, 2.5 µg mEGFP-pDx, pmScarlet-pDx, pmScarlet3-pDx (189754, Addgene), pmScarlet-I3-pDx (189756, Addgene), pmCherry-pDx or pmFusionRed-pDx was transfected into HeLa cells cultured in T25 flasks. After approximately 4 h, the medium was refreshed. Cells were cultured as described under general methods. Cells were passaged at day 2. At day 2 trypsinized control mEGFP cells were mixed with each of the RFP transfected cells. From the five resulting cell mixtures, 4–5 biological replicates were subsequently grown in T25 flasks and passaged on day 4 and on day 6. During passaging on day 2, 4 and 6, two aliquots of (mixed) trypsinized cells were transferred to glass-bottomed 24-well plates supplemented with 0.5 ml culture medium. After 4–5 h of incubation at 37 °C under 7% humidified CO_2 atmosphere, the 24-well plates were analyzed for the number of cells displaying green and red fluorescence by fluorescence microscopy, amounting to 8–10 red/green cell number ratios per time point per RFP. For microscopy, the same setup was used as described in the 'Brightness in mammalian cells' section. For GFP detection a 470 nm LED and

for RFP detection a 555 nm LED (SpectraX, Lumencor) was used. The excitation light from these LEDs was passed through 470/24 or 550/15 nm bandpasses, respectively. A quad band cube (MXU 71640, Nikon) was used. Emission was additionally filtered with a 527/70 or 593/46 nm bandpass (both from Semrock) placed in an optical filter changer (Lambda 10-B, Sutter instrument). For the green and red detected channels, the effective excitation and emission bands were green, 458–483 nm excitation and 492–541 nm emission; and red, 543–558 nm excitation and 570–616 nm emission. A ×10 CFI Plan Apochromat NA 0.45 (Nikon MRD00105) objective was used. Images were acquired on an ORCA-Flash4.0 V2 Digital CMOS camera (C11440-22CU, Hamamatsu Photonics). For each well a 12 × 12 tile of images of 512 × 511 pixels each was acquired using a central ROI of 1,024 × 1,022 pixels with 2 × 2 binning and automated image stitching with 10% overlap, resulting in a final image size of two channels of 5,300 × 5,300 pixels corresponding to a 6.84 × 6.84 mm imaged area in each well. LED power was 50 % and 20% for 470 nm and 555 nm LEDs for the green and red images, respectively. Integration time per image was 100 ms, for each exposure. Between 100 and 3,000 fluorescent cells were counted per well for each color using an automated ImageJ macro. Briefly this macro first reduced noise, performed a background correction and applied a threshold intensity, after which individual cells were automatically counted using the analyze particles ImageJ command. The threshold intensity for the green channel was identical for all analyzed samples and the threshold intensity for the red channel was different for each RFP to account for differences in cellular brightness, but identical for samples from different days. The effective cellular brightness of the different RFPs was determined as described under brightness mammalian cells by analyzing HeLa cells 48 h after transfection with pDress constructs driving expression of mTurquoise2 and the respective RFPs in a 1:1 ratio. The relative brightness and RFP thresholds were 1.307 for mScarlet, 1.899 for mScarlet3, 1.872 for mScarlet-I3, 0.331 for mCherry and 0.298 for FusionRed. This resulted in final thresholds of 24 counts for cells expressing GFP and 100 times the above relative brightness values for the RFP channel thresholds. For each sample (RFP mixture, time point and replicate) the ratio of red fluorescent cells over green fluorescent cells was calculated, normalized to the ratio obtained at day 2 (to correct for possible differing transfection efficiencies) and displayed.

Structure determination

A batch of mScarlet3 protein sample was specifically expressed and purified for crystallization purposes.

Protein expression. Bacterial transformation of the pDX vector was achieved in *E. coli* BL21 (DE3) (Invitrogen) and incubated overnight at 30 °C on kanamycin (30 µg ml^{-1})-selective LB-agar plates. A starting culture of 100 ml LB supplemented with kanamycin (30 µg ml^{-1}) was grown overnight at 37 °C under agitation (165 r.p.m.). One liter LB supplemented with kanamycin (30 µg ml^{-1}) was inoculated with 10 ml starting culture, then grown at 37 °C, 145 r.p.m. until the OD (600 nm) reached 0.6. Protein expression was then induced with L-rhamnose at a final concentration of 0.2% and grown overnight at 20 °C at 145 r.p.m.

Purification. Cultures were centrifugated at 4,000*g* for 30 min at 4 °C. The pellets were then resuspended in 25 ml lysis buffer (50 mM Tris, pH 8.0, 300 mM NaCl, 10 mM imidazole, 20 mM $MgSO_4$, one tablet of the EDTA-free protease inhibitor cocktail complete (Roche) and 400 µg ml^{-1} DNase) per liter of culture, flash-frozen and stored at −80 °C overnight. Thawed pellets were sonicated and cell debris were centrifuged at 18,000*g* for 45 min at 4 °C. The clarified lysate was then loaded on nickel affinity Histrap HP 1 ml (Cytiva) column for protein purification. Proteins were eluted against an imidazole buffer (20 mM Tris, pH 8.0, 200 mM NaCl and 500 mM imidazole) with isocratic elution (5–500 mM imidazole in 10% increments). The final purification step consisted in a size exclusion chromatography using a HiPrep 16/60 Sephacryl 100S HR column (Cytiva) against a 20 mM Tris, pH 8.0, buffer. Purified mScarlet3 proteins were concentrated to 15 mg ml^{-1} using an Amicon 15 (10 kDa cutoff, Merck Millipore) for further crystallization assays.

Protein crystallization and crystal collection. Crystallization conditions were set up in 96-well CrystalDirect plates using commercial screens available at the HTX laboratory crystallization platform (https://htxlab.embl.fr/, EMBL Grenoble). These plates are suitable for automated crystal collection based on photoablation of the cover film[21]. A condition consisting of 0.1 M NaCl, 0.1 M HEPES, pH 7.5 and 1.6 M ammonium sulfate in a mother liquor:protein ratio of 1:2 yielded a crystal of 800 × 400 × 200 µm^3. The position of the crystal was marked using the Crystal Harvesting Interface provided within the plate viewing function of the CRIMS (Crystallographic Information Management System) system and used for automated collection and flash-cooling of the sample. Cryoprotection was achieved by removing excess of mother liquor around the crystal by aspiration before crystal collection without addition of any cryoprotectant molecule.

Data collection, processing and structure refinement. The data collection was performed at 100 K at beamline ID30B of the ESRF[22] using an X-ray detector Pilatus3 6M (Dectris). Data were integrated using the automated processing pipeline[22] accessible in the extended Laboratory Information Management System ISPyB (https://exi.esrf.fr/)[23]. The best data integration was obtained with the XDSAPP pipeline and yielded structure factors in the $P2_12_12_1$ space group at 1.33 Å resolution using a $CC_{1/2}$ resolution cutoff of 0.5. Data collection statistics are in Supplementary Table 2. The structure was solved by the molecular replacement method with PHASER v.2.8.3 (ref. [24]) using the previously determined mScarlet structure (Protein Data Bank (PDB) accession code 5LK4)[9]. The asymmetric unit is composed of two molecules of mScarlet3. Cycles of structure refinement and model rebuilding upon electron density map inspection were performed using REFMAC v.5.8.0267 (ref. [25]) and COOT[26], respectively. In the Ramachandran plot, 98.3% of residues were in the favored region, 1.7% were in the allowed region and 0.0% were outliers. Only 0.5% of side chain rotamers were outliers. Structure refinement statistics are in Supplementary Table 2. The structure of mScarlet3 at pH 7.5 has been deposited in the PDB under accession code 7ZCT.

Zebrafish larvae experiments

Wild-type zebrafish (AB) larvae were maintained at 28 °C in E3 medium. Injections were performed on fertilized zebrafish eggs at the one-cell stage.

Episomal expression was assessed by injecting pDRESS_mTurquoise2_spatial-linker-P2A_mScarlet (189752, Addgene) and pDRESS_mTurquoise2_spatial-linker-P2A_mScarlet3 (130509, Addgene)[11] at a concentration of 250 ng µl^{-1}. After 24 h, the larvae were fixed in 4% paraformaldehyde and subsequently analyzed on a confocal microscope with a ×40 PLAN Apochromat 1.3 NA objective (SP8X, Leica Microsystems). A white-light laser set at 405 nm (7.5%) and 569 nm (25%) was used to excite mTurquouise2 (Em 450–525) and mScarlet or mScarlet3 (Em 580–655 nm), respectively. For quantification, the relative fluorescence intensity of the mScarlet(3) channel compared to the mTurquoise2 channel was calculated for 35 ROIs per construct.

Expression of mScarlet3 in the pancreas was allowed by placing mScarlet3 under the control of the ElastaseA promoter in a Tol2 backbone and co-injecting this with Tol2 transposase mRNA, both at 250 ng µl^{-1} (refs. [27–29]). The Tol2 plasmid was a kind gift from Dr Kawakami, Japan[28,30]. After 24 h, pigment formation was inhibited by adding 1-phenyl 2-thiourea to a final concentration of 0.2 mM. Timelapse imaging was performed on a single-plane illumination microscope with a ×10 PLAN Apochromat 0.5 NA detection objective

(LS7, Zeiss) at 15-min intervals for 12 h with a Z-stack of 79 frames taken at each time point with 1.73-µm intervals using Zeiss Zen Black v.3.1. Here, the zebrafish larva was illuminated through the ventral and dorsal sides with a 561 laser and detection was conducted through a 575–615 nm bandpass filter with a camera set at 120 ms exposure time. For illustration (Fig. 2j and Supplementary Video 5), only the images originating from ventral sided illumination were used. A maximum intensity projection of 21 frames in Z, surrounding a dividing cell, was generated and time alignment with linear interpolation and subsequent cropping was performed to account for drift over time (Zen blue v.3.0, Zeiss). The image represents a single experiment.

For the analysis of H2B-mScarlet3 in zebrafish larvae, mScarlet3 cDNA was cloned in frame with histone 2B and subsequently cloned in the pCS2^{+} backbone containing the SP6 promotor. Capped RNA was in vitro transcribed using the mMESSAGE mMACHINE SP6 Transcription kit (Invitrogen, AM1340) and subsequently cleaned up using MEGAclear Transcription Clean-Up kit (Invitrogen, AM1908). Zebrafish embryos were micro-injected with the capped RNA in the one-cell stage and incubated in E3 medium containing 0.2 mM N-phenylthiourea (Sigma-Aldrich, P7629) to inhibit pigment formation. At 30 h after fertilization the zebrafish embryos were sedated using 0.2 g l^{-1} ethyl 3-aminobenzoate (Tricaine, MS-222) (Sigma-Aldrich, E10521). For Fig. 2k and Supplementary Videos 6 and 7, imaging was performed on a single-plane illumination microscope using a ×10 Plan Apochromat 0.5 NA detection objective (LS7, Zeiss). Z-stack images were recorded at 1-µm intervals over 309 frames with 5-min intervals for 6 h. Here, the zebrafish embryo was excited from the ventral and dorsal sides with a 561 nm laser and detection of the sagittal plane was conducted using a 585 nm long-pass filter with the camera set at 100 ms exposure time (this was the first experiment that was immediately successful).

Reporting summary

Further information on research design is available in the Nature Portfolio Reporting Summary linked to this article.

Data availability

The data supporting this study are available within the article and the Supplementary Information, including the digital data underlying the figures. Other (raw) data supporting this study are available from the corresponding author upon reasonable request. Plasmids constructed in this study, their maps and sequences were deposited to the non-profit organization Addgene ID 189752-189779. The mScarlet3 crystal structure was deposited at the PDB under accession code 7ZCT. Source data are provided with this paper.

Code availability

Image analysis was performed in ImageJ/Fiji using macros described previously[11]. The codes are available at GitHub (https://github.com/molcyto/MC-FLIM-Petri-dish; https://github.com/molcyto/MC-Ratio-Petri-dish; https://github.com/molcyto/MC-FLIM-96-wells; https://github.com/molcyto/MC-Ratio-96-wells; https://github.com/molcyto/MC-Bleach-96-wells).

References

16. Gross, L. A., Baird, G. S., Hoffman, R. C., Baldridge, K. K. & Tsien, R. Y. The structure of the chromophore within DsRed, a red fluorescent protein from coral. *Proc. Natl Acad. Sci. USA* **97**, 11990–11995 (2000).
17. Shagin, D. A. et al. GFP-like proteins as ubiquitous metazoan superfamily: evolution of functional features and structural complexity. *Mol. Biol. Evol.* **21**, 841–850 (2004).
18. Vermeer, J. E. M., van Munster, E. B., Vischer, N. O. & Gadella, T. W. J. Jr. Probing plasma membrane microdomains in cowpea protoplasts using lipidated GFP-fusion proteins and multimode FRET microscopy. *J. Microsc.* **214**, 190–200 (2004).
19. Aslantürk, Ö. S. in *Genotoxicity—A Predictable Risk to Our Actual World* (InTech, 2018).
20. Dabbaghi, M., Hashemi, K., Oskuee, R. K. & Afkhami-Goli, A. Reverse relation between cytotoxicity and polyethylenimine/DNA ratio, the effect of using HEPES-buffered saline (HBS) medium in gene delivery. *Toxicol. Vitr.* **83**, 105414 (2022).
21. Cipriani, F. et al. CrystalDirect: a new method for automated crystal harvesting based on laser-induced photoablation of thin films. *Acta Crystallogr D Biol. Crystallogr.* **68**, 1393–1399 (2012).
22. McCarthy, A. A. et al. ID30B - a versatile beamline for macromolecular crystallography experiments at the ESRF. *J. Synchrotron Radiat.* **25**, 1249–1260 (2018).
23. Delagenière, S. et al. ISPyB: an information management system for synchrotron macromolecular crystallography. *Bioinformatics* **27**, 3186–3192 (2011).
24. McCoy, A. J. et al. Phaser crystallographic software. *J. Appl. Crystallogr.* **40**, 658–674 (2007).
25. Murshudov, G. N. et al. REFMAC5 for the refinement of macromolecular crystal structures. *Acta Crystallogr. D Biol. Crystallogr.* **67**, 355–367 (2011).
26. Emsley, P., Lohkamp, B., Scott, W. G. & Cowtan, K. Features and development of Coot. *Acta Crystallogr. D Biol. Crystallogr.* **66**, 486–501 (2010).
27. Kawakami, K. Tol2: a versatile gene transfer vector in vertebrates. *Genome Biol.* **8 Suppl 1**, S7 (2007).
28. Kawakami, K. et al. A transposon-mediated gene trap approach identifies developmentally regulated genes in zebrafish. *Dev. Cell* **7**, 133–144 (2004).
29. Wan, H. et al. Analyses of pancreas development by generation of gfp transgenic zebrafish using an exocrine pancreas-specific elastaseA gene promoter. *Exp. Cell. Res.* **312**, 1526–1539 (2006).
30. Urasaki, A., Morvan, G. & Kawakami, K. Functional dissection of the Tol2 transposable element identified the minimal *cis*-sequence and a highly repetitive sequence in the subterminal region essential for transposition. *Genetics* **174**, 639–649 (2006).

Acknowledgements

We are grateful to R. Breedijk (Amsterdam) for assistance and maintenance of the LCAM microscopes and to S. Engilberge (Grenoble) for assistance in drawing mScarlet3 structural figures. Part of the work was performed in the UMCG Microscopy and Imaging Center. This work was supported by a grant from the French Agence Nationale de la Recherche (ANR-17-CE11-0013 to J.D.).

Author contributions

T.W.J.G. designed and supervised the project. L.v.W. and J.S. performed the mutagenesis experiments. L.v.W. prepared bacteria, purified proteins, cultured and transfected mammalian cells. T.W.J.G. performed and analyzed the spectroscopic characterization and cellular imaging experiments. M.A.H. performed and analyzed the TCSPC experiments. A.H.G.W. and B.N.G.G. performed and analyzed the zebrafish experiments. S.A., J.D. and A.R. purified mScarlet3 for crystallization, crystallized mScarlet3 and solved and analyzed the crystal structure. T.W.J.G. and A.R. wrote the manuscript with input from all authors.

Competing interests

The University of Amsterdam has applied for a European Patent (EP 33108) and international PCT Patent (WO 35192; patents pending) on 'Improved variants of monomeric scarlet red fluorescent protein' with T.W.J.G. and L.v.W. as inventors. All other authors have no competing interests.

Additional information

Extended data is available for this paper at https://doi.org/10.1038/s41592-023-01809-y.

Supplementary information The online version contains supplementary material available at https://doi.org/10.1038/s41592-023-01809-y.

Correspondence and requests for materials should be addressed to Theodorus W. J. Gadella Jr.

Peer review information *Nature Methods* thanks the anonymous reviewers for their contribution to the peer review of this work. Primary Handling Editor: Nina Vogt, in collaboration with the *Nature Methods* team.

https://doi.org/10.1038/s41592-023-01809-y

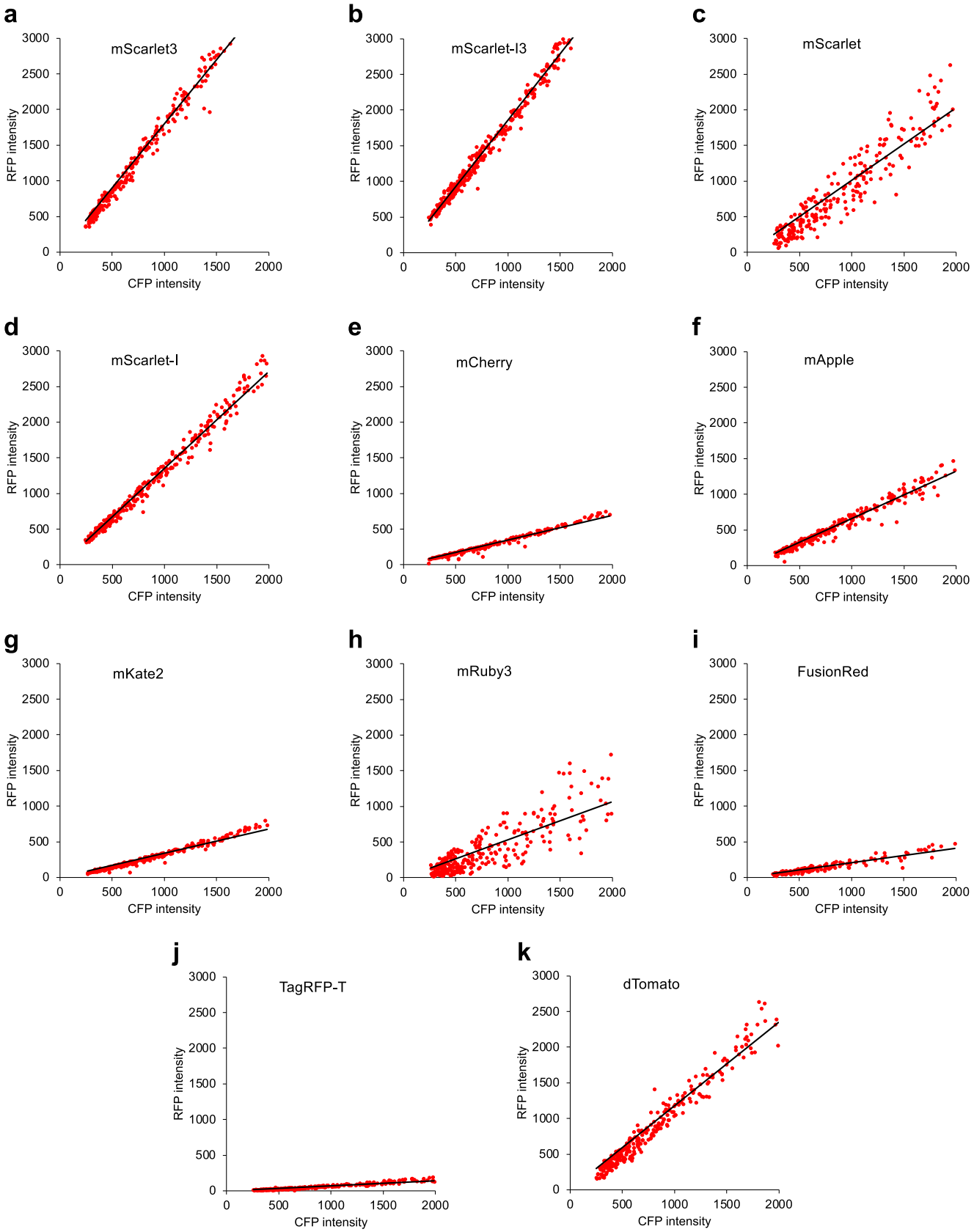

Extended Data Fig. 1 | See next page for caption.

https://doi.org/10.1038/s41592-023-01809-y

Extended Data Fig. 1 | Brightness of RFPs in HeLa cells 24 h after transfection. For each RFP an mTurquoise2 construct was coexpressed in cells in a 1:1 molecular ratio. The average red fluorescence and cyan fluorescence was quantified for each cell (red data points). a mScarlet3 n = 231, b mScarlet-I3 n = 303, c mScarlet n = 238, d mApple n = 266, e mCherry n = 272, f mScarlet-I n = 303, g mKate2 n = 294, h mRuby3 n = 275, I FusionRed n = 156, j TagRFP-T n = 320, and k dTomato n = 268. The red fluorescence values were corrected for spectral throughput of the microscope (correcting for instrument-dependent excitation and detection efficiencies of the different RFPs). The slopes of the linear regression line that is forced the origin was used for calculating the relative brightness of the RFPs (as compared to mScarlet) and indicated in Extended Data Table 1 and Fig. 1d. The slope was calculated as $\sum RC/\sum C^2$ in which R is the RFP intensity value of a single cell (vertical axes) and C is the CFP intensity of the same cell (horizontal axes). The standard error of the slope (indicated in Fig. 1d and Extended Data Table 1) was calculated as $\mathrm{Sqrt}((\sum R^2-(\sum RC)^2/\sum C^2)/((n-1)\sum C^2))$. In which n is the number of cells.

https://doi.org/10.1038/s41592-023-01809-y

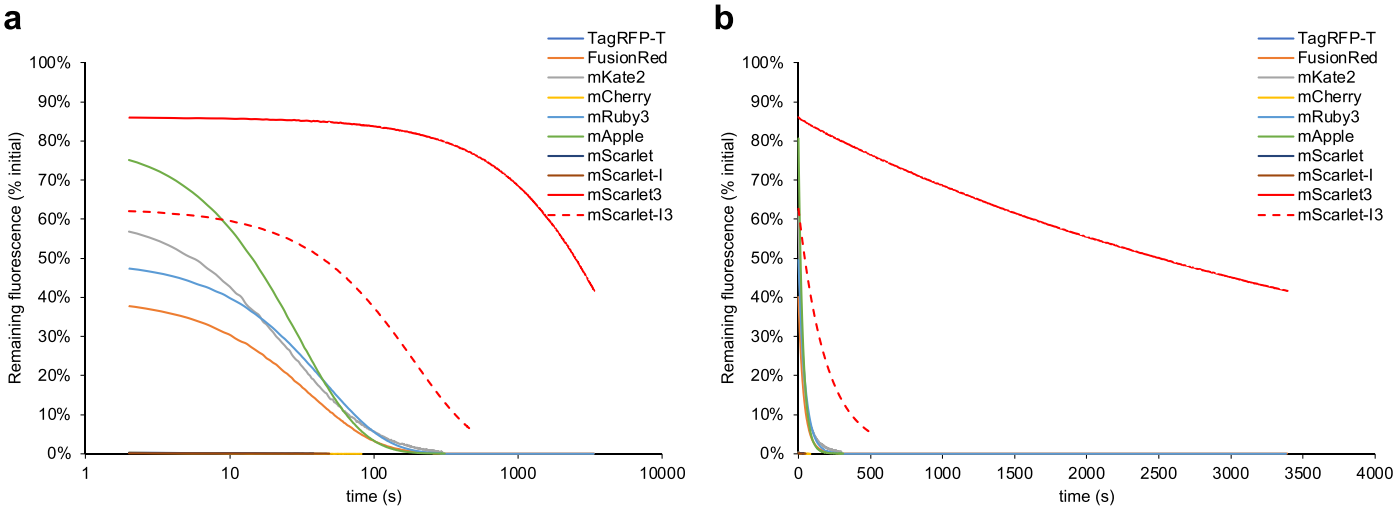

Extended Data Fig. 2 | Alkaline denaturation speed of diverse purified RFPs at pH 13.5. a: logarithmic time axis, **b**: normal time axis.

https://doi.org/10.1038/s41592-023-01809-y

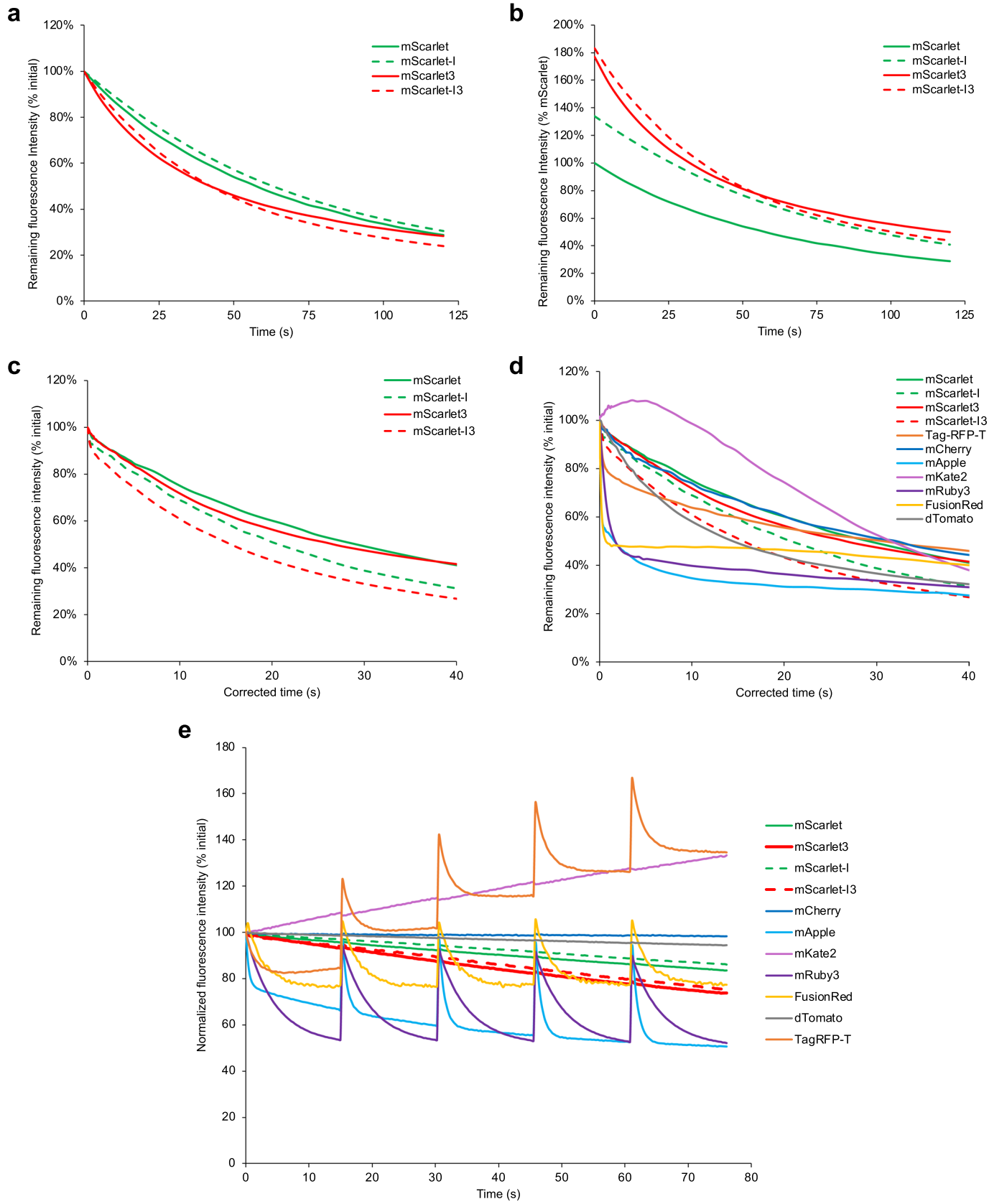

Extended Data Fig. 3 | See next page for caption.

https://doi.org/10.1038/s41592-023-01809-y

Extended Data Fig. 3 | Photostability of RFP variants. a: Wide-field bleaching of mScarlet variants without time-axis correction, **b**: same data as a) but y-axis scaled according to cellular brightness; **c**: confocal bleaching of mScarlet variants; **d**: confocal bleaching of mScarlet variants and other RFPs. In order to fairly compare the photostability of different RFP variants under confocal imaging conditions, the time axis is corrected in c and d for spectral properties relative to mScarlet to mimic an identical overall emission rate (photons/s) for all RFPs at the start of the experiment. **e**: Blue light-induced photochromicity of RFP variants. The RFP variants were expressed in HeLa cells and continuously exposed with 550 nm excitation light. At t = 15, 31, 46 and 52 s, the 550 nm excitation light interrupted by a brief excitation at 470 nm for 1 s (not recorded on time axis) after which the 550 nm excitation was continued. The sudden increase after blue light excitation is caused by photochromic behavior.

https://doi.org/10.1038/s41592-023-01809-y

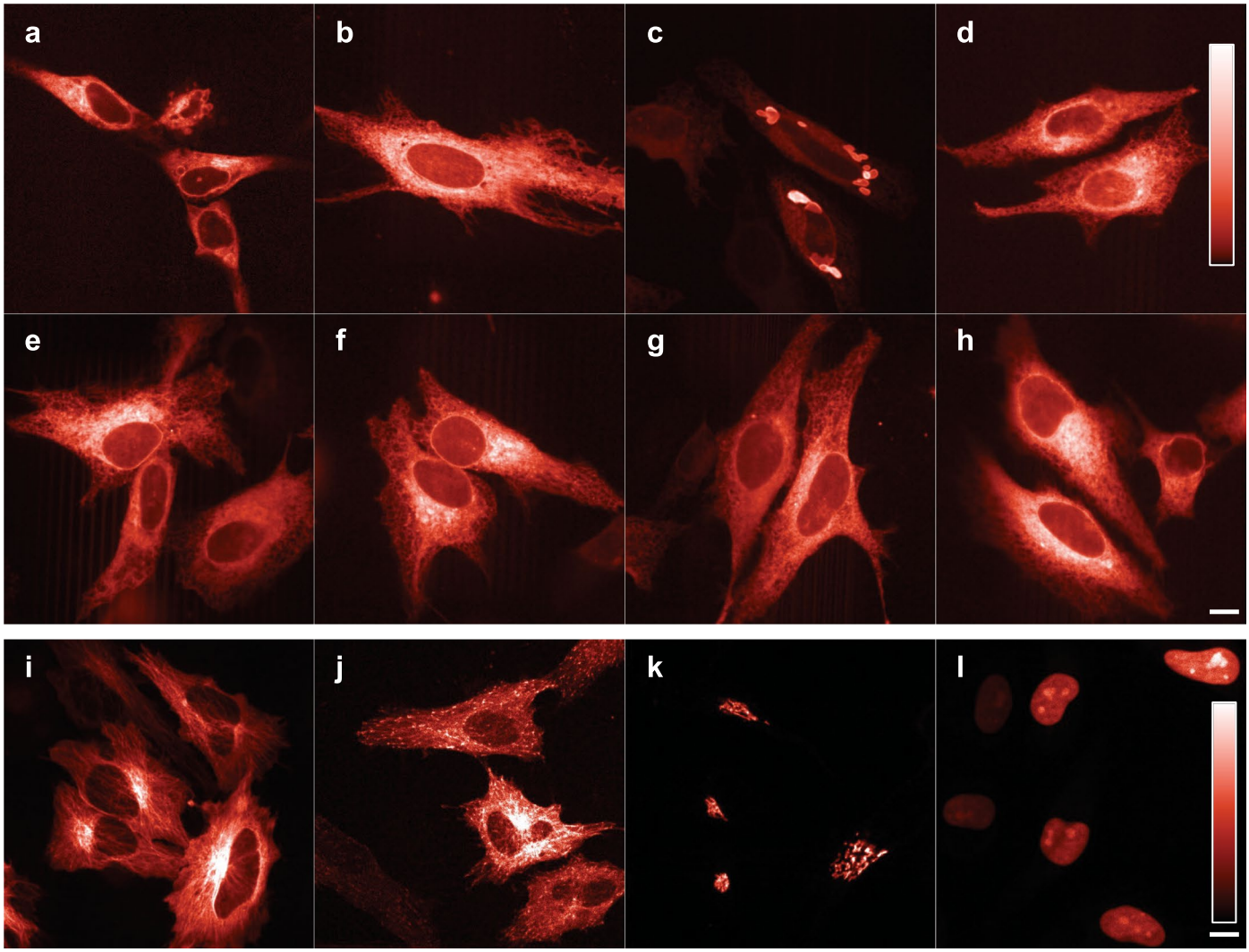

Extended Data Fig. 4 | Evaluation of RFPs as fusion tag in HeLa cells. a-h: representative images of selected Cyterm-RFP fusions in HeLa cells 24 h after transfection. **a** FusionRed, **b** mScarlet3; **c** TagRFP-T; **d** mCherry; **e** mScarlet-I3; **f** mScarlet-I3-NCwt; **g** mScarlet-I; **h** mScarlet. For a-h bar is 10 µm and the fluorescence intensities were pseudo-colored between minimum and maximum intensities according to the mScarlet lookup table as indicated in image d and subsequently gamma-corrected (value 0.5, including the lookup table) to better visualize the low intensity areas. For cell numbers imaged and evaluated see Extended Data Table 1, images shown are representative of these. **i-l**: mScarlet3 as fusion tag for cellular localization studies. mScarlet3 was fused to: **i** alpha-tubulin (microtubule cytoskeleton); **j** EB3 (+ends of microtubules); **k** Giantin (Golgi apparatus); and **l** a 3x repeated nuclear localization signal (NLS) (nuclei) and expressed in HeLa cells. For i-l bar is 10 µm and the fluorescence intensity was pseudo-colored between minimum and maximum fluorescence according to the mScarlet lookup table indicated in l. Micrographs shown in i-l are representative of at least 4 images made from 2 independent transfections.

https://doi.org/10.1038/s41592-023-01809-y

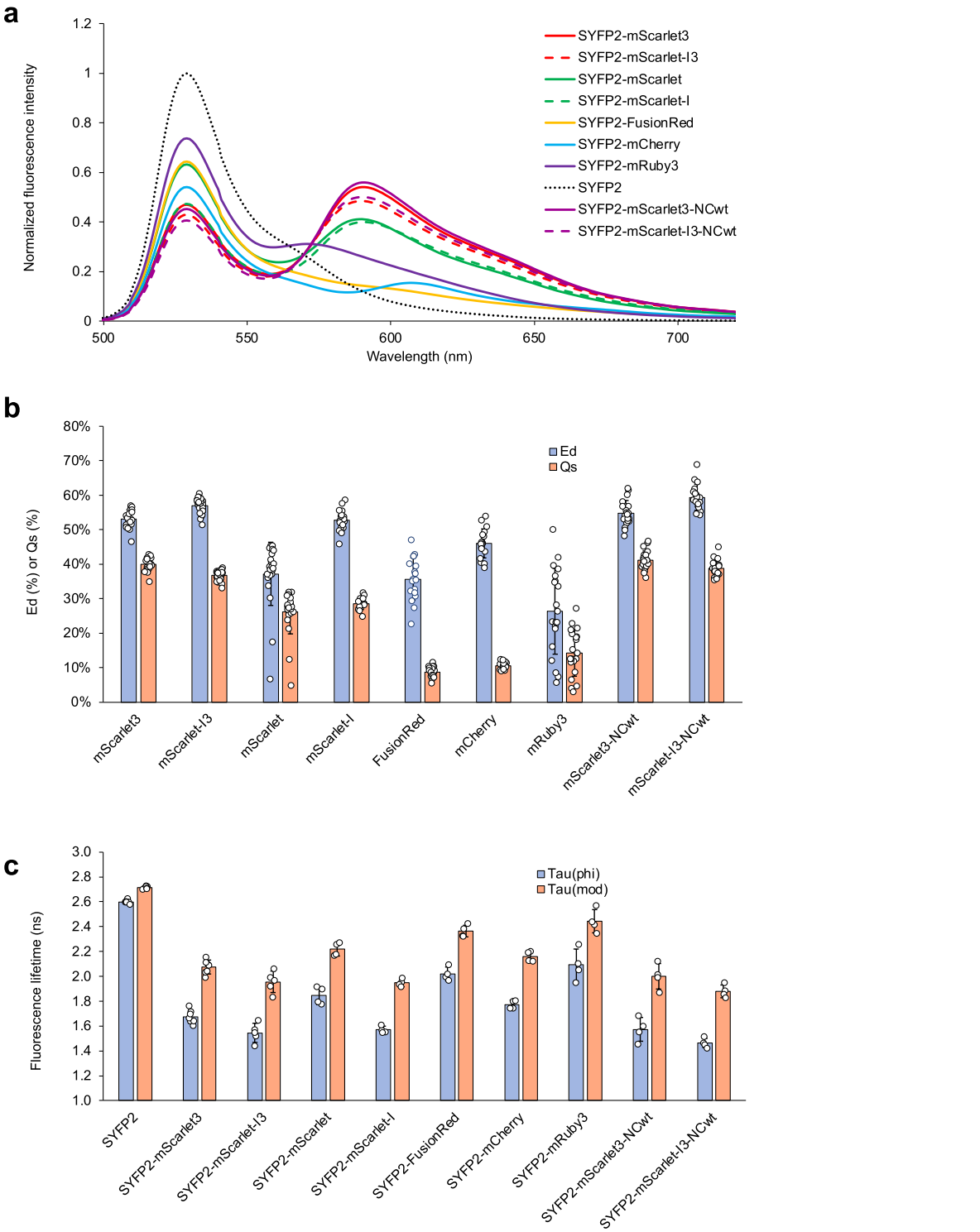

Extended Data Fig. 5 | FRET in HeLa cells expressing SYFP2 alone or SYFP2-RFP fusion proteins. a. Average FRET spectra from HeLa cells expressing SYFP2 alone or SYFP2-RFP fusion proteins. All spectra were normalized to the unquenched SYFP2 donor. **b**. Quantification of FRET spectra from a. E (blue bars) represent the energy transfer efficiency (average ± sd), and Qs (red bars) depict the sensitized emission quantum yield (average ± sd). Qs is defined as the number of sensitized emission quanta emitted by the RFP acceptor divided by the number of quanta absorbed by the SYFP2 donor and is calculated by Qs=E·Qa, in which Qa is the acceptor quantum yield of fluorescence. Qs is not dependent on the emission spectra and is proportional to the integrated acceptor sensitized emission signal. Each data point represents quantitative unmixing analysis of a single cell spectrum, 18–25 single cell spectra were recorded for each condition. **c**. SYFP2 fluorescence lifetime of HeLa cells expressing SYFP2 alone or SYFP2-RFP fusion proteins as determined by frequency-domain FLIM. Tau(phi) (red bars) is the average lifetime estimated from the phase shift (± sd), Tau(mod) (blue bars) is the average fluorescence lifetime estimated from the demodulation (± sd). For c each data point represents the average lifetime of an image with 4–20 individual cells, 4–6 FLIM recordings were done for each condition.

https://doi.org/10.1038/s41592-023-01809-y

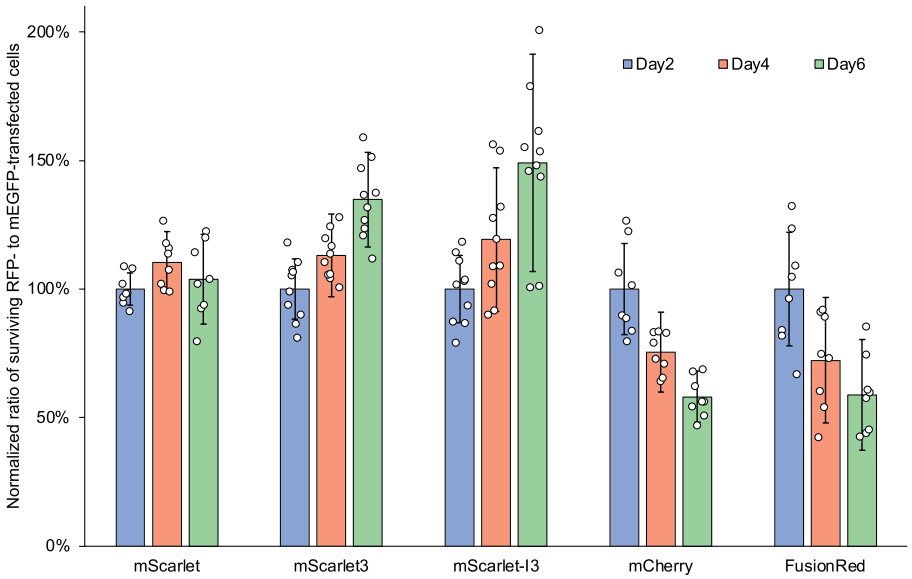

Extended Data Fig. 6 | Relative cell viability of RFP transfected cells. mEGFP and RFPs were transfected separately into HeLa cells at day 0. At day 2 each of the RFP transfected cells were split and mixed with mEGFP transfected cells. At days 4 and 6 the cell mixtures were resplit. At days 2, 4 and 6 after (4–5 h after splitting/mixing) the number of RFP and mEGFP expressing cells in the mixtures was scored. The ratio of RFP to mEGFP expressing cells was normalized to that obtained at day 2 to correct for bias in transfection efficiencies. For each RFP 8-12 technical replicates (depicted as individual data points) were measured. The average normalized ratio of red to green cell numbers ± sd is indicated.

https://doi.org/10.1038/s41592-023-01809-y

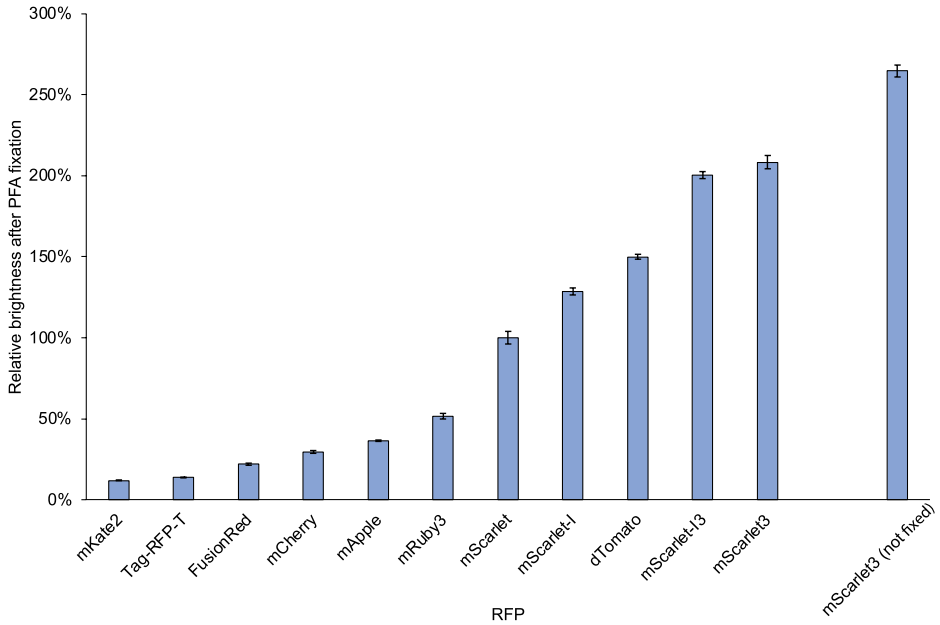

Extended Data Fig. 7 | Brightness of RFPs in mammalian cells after fixation relative to mScarlet. Indicated is the average relative brightness (± sd), corrected for spectral throughput determined from single cell red to cyan ratios and linear regression (though the origin) like in Extended Data Fig. 1.

https://doi.org/10.1038/s41592-023-01809-y

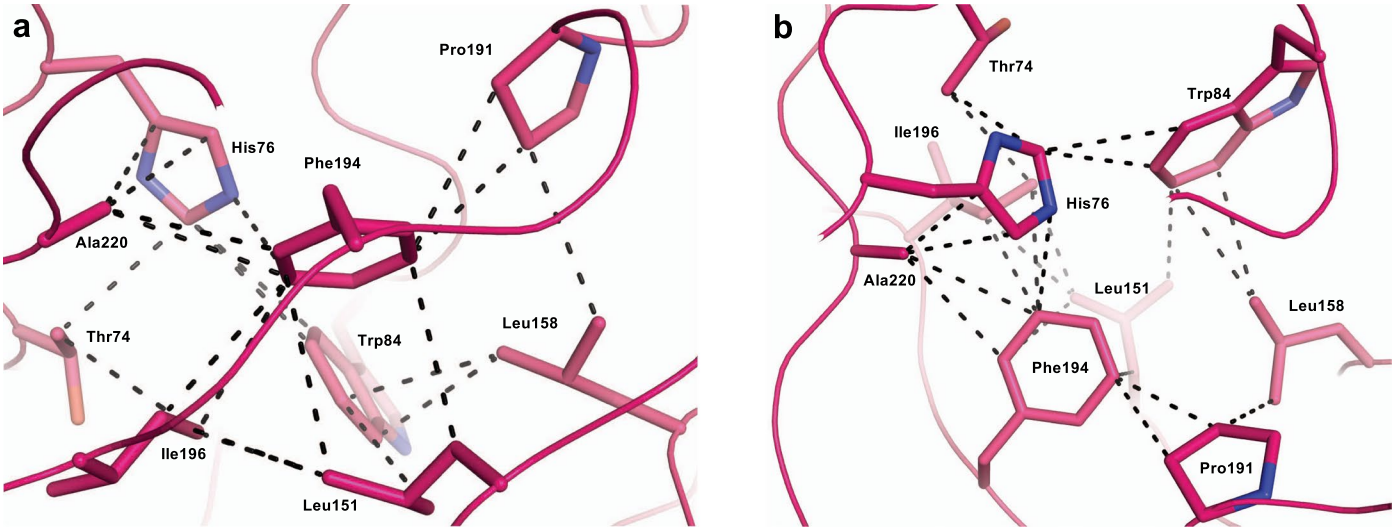

Extended Data Fig. 8 | Illustration of the potential van der Waals interactions between 9 residues of mScarlet3 near the surface of one head of the β-barrel. Residues belong to the central α-helix traversing the β-barrel (Thr74), to the α-helix capping one head of the β-barrel (Trp84), to the loop linking the latter helices (His76), to the 7th strand (Leu151), to the 8th strand (Leu158), to the loop bridging the 9th and 10th strands (Pro191), to the 10th strand (Phe194, Ile196), to the 11th strand (Ala220). Potential van der Waals interactions (dashed black lines) are highlighted by inter-carbon atom distances below 4.0 Å. **a**. View from the side of the β-barrel. The set of vdW interactions forms a crown-like structure.**b**. 90° view (from the barrel head) showing residues organized in three layers: the main one is formed of residues Thr74, Trp84, Leu158, Phe194 and Ala220, with residues His76 and Pro191 ahead of this layer, and residues Leu151 and Ile196 behind it.

https://doi.org/10.1038/s41592-023-01809-y

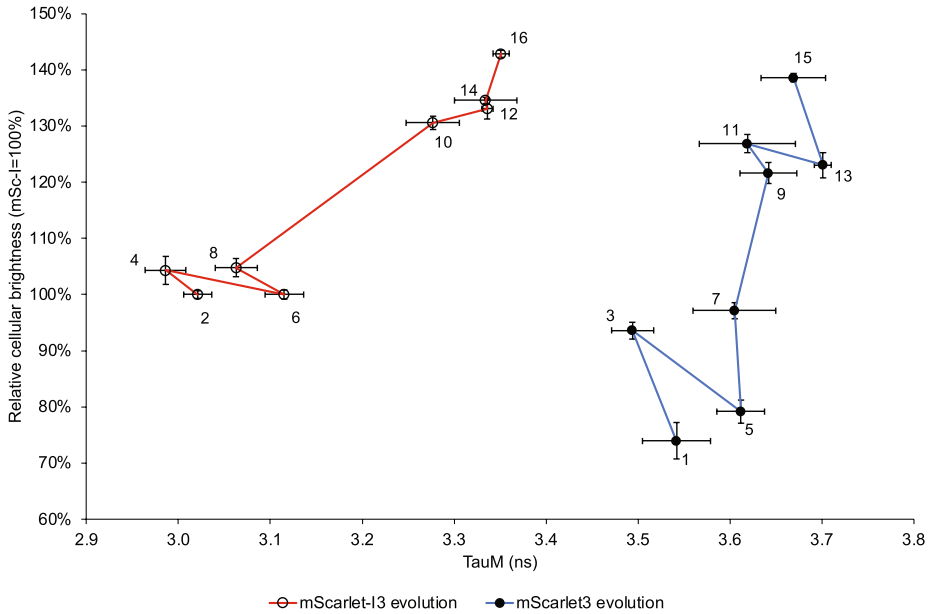

Extended Data Fig. 9 | Evolution path for mScarlet3 (seq-id #15) and mScarlet-I3 (#16) from mScarlet (#1) and mScarlet-I (#2), respectively. The numbers correspond with the sequence IDs in Supplementary Fig. 1. The horizontal axis depicts the (modulation) fluorescence lifetime as determined in live HeLa cells ~ 24 h after transfection and corresponds with intrinsic brightness (more to the right is better), and the vertical axis depicts the cellular brightness (higher is better) normalized to mScarlet-I. F. Vertical error bars are SD of the slope of the line fitted to the red to cyan cellular ratios (of 22–77 cells, for example see Extended Data Fig. 1) or the average modulation lifetime of the mScarlet variant in HeLa cells (from 3 individual FLIM recordings with > 5 cells each).

https://doi.org/10.1038/s41592-023-01809-y

Extended Data Table 1 | Properties of red fluorescent proteins

	Spectroscopic Characteristics												Brightness		Photostability			Maturation		Stability pH13.5		Ratio FRET	Monomeric Assay		
	Abs max[a] (nm)	Em max[b] (nm)	ε[c] 10^3 $M^{-1}cm^{-1}$	QY[d] (%)	τ_1[e] (ns)	τ_2[f] (ns)	α_1[g] (%)	χ^{2}[h]	τ_{avg}[i] (ns)	τ_M(cells)[j] (ns)	pK_a[k]	n[l]	EC*QY[m]	Cells[n] % 24h	WF $t_{1/2}$[o] (s)	Confocal $t_{1/2}$[p] (s)	PC[q] %	Accum[r] (% mSc-I)	delay[s] (h)	I_0[t] (%)	$t_{1/2}$[u] (min)	Sens em[v] (%)	Correct ER[w] (%)	# OSER[x] (%)	cells[y] n
mScarlet3	569	592	104±1	75.1±1	3.96±0.01	x	100	1.15	3.96	3.67±0.04	4.5±0.1	0.70+0.04	78±1	177±1	52	27	<1%	94.9±0.5	0.6±0.2	86	45.6	140±7	85	7	139
mScarlet-I3	568	592	105±2	64.5±1.1	3.64±0.01	x	100	1	3.64	3.35±0.01	4.2±0.1	0.70±0.04	69±2	183±1	47	16	1.1±0.3%	113.5±0.3	0.0±0.2	63	2.24	129±5	87	5	204
mScarlet-I3-NCwt	568	592	102±0.5	65.3±0.8	3.63±0.01	x	100	1.25	3.63	3.33±0.03	4.2±0.1	0.76±0.16	68±1	177±1		15		115±1	-	70	2	136±9	87	0	61
mScarlet	569	593	*100±3*	*70.4±0.8*	*3.86±0.01*	*x*	*100*	*1.12*	*3.86*	3.53±0.01	*5.3±0.2*	*0.79±0.22*	*71±2*	100±1	62	29	<1%	60±1	2.3±0.6	<0.5	x	92±23	92	8	39
mScarlet-I	569	594	*104±3*	*54±4*	*3.52±0.02*	*1.67±0.04*	*76±1*	*1.11*	*3.08*	3.01±0.04	*5.4±0.4*	*0.52±0.19*	*57±4*	134±1	55	21	<1%	100.0±0.4	0.1±0.2	<0.5	x	100±6	84	8	80
mRuby3	557	591	127±0.3	54±1	2.80±0.01	x	100	1.04	2.80	2.49±0.02	*4.8*		69±1	53±1	*	*	42±1%	32±1	5.2±1.0	50	0.53	50±24	0	24	17
mKate2	588	631	*63±3*	*39±1*	*2.47±0.01*	*x*	*100*	*1.21*	*2.47*	2.53±0.01	*5.4*		*25±1*	33.5±0.3	96	32	<1%	57.3±0.3	1.2±0.4	62	0.58		56	12	68
Tag-RFP-T	556	585	*110±7*	*48±1*	*2.66±0.02*	*1.44±0.06*	*72±3*	*1.12*	*2.32*	2.44±0.02	*4.6*		*53±2*	7.1±0.1	*	*	27±3%	5.6±0.1	1.8±0.4	<0.5	x		31	66	182
mCherry	586	610	*88±1*	*23±1*	*1.28±0.03*	*2.00±0.07*	*71±0*	*1.08*	*1.49*	1.56±0.01	*<4.5*		*20±1*	34.2±0.2	55	32	<1%	70.9±0.4	0.7±0.3	<0.5	x	37±3	82	18	87
FusionRed	575 *580ex*[z]	605 *608*[z]	93 *94.5*[z]	24±1 *19*[z]	1.58±0.03	2.72±0.15	84±4	1.01	1.76	1.71±0.03	*4.6*[z]		22 *18*[z]	20.3±0.3	*	*	26±0.2%	37.6±0.6	3.1±0.7	40	0.48	31±5	67	4	99
dTomato	555	583	*90±1*	*69±1.3*	*3.47±0.01*	*1.21±0.07*	*95±0*	*1.36*	*3.36*	3.28±0.02	*4.7*		*62±1*	116±1	154	14	<1%	112±2	1.6±0.4	<0.5	x		17	82	266

[a]Absorbance maximum. [b]Emission maximum. [c]Extinction coefficient at maximum absorbance. [d]Quantum yield. [e]Fluorescence lifetime component 1. [f]Fluorescence lifetime component 2. [g]Amplitude of fluorescence lifetime component 1. [h]Chi-square fluorescence lifetime fit. [i]Average fluorescence lifetime weighed by amplitude. [j]Modulation lifetime in cells. [k]Apparent pKa value. [l]Hill coefficient. [m]Calculated intrinsic brightness, product of extinction coefficient and quantum yield. [n]Brightness in mammalian cells normalized to mScarlet-I. [o]Time in seconds to half the emission rate under wide-field conditions. [p]Time in seconds to half the emission rate under confocal spinning disk conditions. [q]Percentage of photochromic behavior. [r]Accumulation in cells normalized to mScarlet-I (brightness in cells divided by intrinsic brightness). [s]Apparent delay time of maturation relative to mTurquoise2 in mammalian cells. [t]Initial fluorescence at pH 13.5 relative to pH 7.4. [u]Time required to reduce fluorescence by 50% at pH 13.5. Sensitized emission by FRET in a RFP-SYFP2 fusion, corrected for direct excitation of donor and acceptor, normalized to mScarlet-I. [w]Percentage of cells with a correct ER labeling upon expressing an Cyterm-RFP fusion. [x]Percentage of cells visible OSER structures upon expressing an Cyterm-RFP fusion. [y]Number of analyzed cells. [z]Values from Semiakina et al.. c,d,e,f,j,k,n,m,n,q,r,s ± standard deviation, or value cited from literature. Values in *Italics* from Bindels et al.[9].

nature research

Corresponding author(s): TWJ Gadella

Last updated by author(s): Nov 25, 2022

Reporting Summary

Nature Research wishes to improve the reproducibility of the work that we publish. This form provides structure for consistency and transparency in reporting. For further information on Nature Research policies, see our Editorial Policies and the Editorial Policy Checklist.

Statistics

For all statistical analyses, confirm that the following items are present in the figure legend, table legend, main text, or Methods section.

n/a	Confirmed	
☐	☒	The exact sample size (*n*) for each experimental group/condition, given as a discrete number and unit of measurement
☐	☒	A statement on whether measurements were taken from distinct samples or whether the same sample was measured repeatedly
☒	☐	The statistical test(s) used AND whether they are one- or two-sided *Only common tests should be described solely by name; describe more complex techniques in the Methods section.*
☒	☐	A description of all covariates tested
☒	☐	A description of any assumptions or corrections, such as tests of normality and adjustment for multiple comparisons
☐	☒	A full description of the statistical parameters including central tendency (e.g. means) or other basic estimates (e.g. regression coefficient) AND variation (e.g. standard deviation) or associated estimates of uncertainty (e.g. confidence intervals)
☒	☐	For null hypothesis testing, the test statistic (e.g. *F*, *t*, *r*) with confidence intervals, effect sizes, degrees of freedom and *P* value noted *Give P values as exact values whenever suitable.*
☒	☐	For Bayesian analysis, information on the choice of priors and Markov chain Monte Carlo settings
☒	☐	For hierarchical and complex designs, identification of the appropriate level for tests and full reporting of outcomes
☒	☐	Estimates of effect sizes (e.g. Cohen's *d*, Pearson's *r*), indicating how they were calculated

Our web collection on statistics for biologists contains articles on many of the points above.

Software and code

Policy information about availability of computer code

Data collection	Data collection: Fluorescence spectra were acquired using a Jasco FP-8500 spectrofluorimeter operated by Jasco SpectraManager (version 2.15). pH-dependent fluorescence intensity was measured with a BioTek FL-600 fluorescence plate reader using KC4 (version 3.0). TCSPC data were acquired using the PicoQuant SymPhoTime (software version 64.2.1). FRET spectra from single cells were acquired using MatLab 6.1 controlling an Hamamatsu ORCA camera using DCAMAPI. Widefield fluorescence microscopy (for measuring ratio's, photobleaching, photochromicity, maturation) was performed using Nikon NIS Elements AR (version 4.51.01 64-bit). FLIM data was acquired using Lambert Instruments LiFLIM software (version 1.2.23). Spinning disk confocal images (localization, OSER, bleaching) were acquired using Nikon NIS Elements AR (version 4.51.01 64-bit). Proloned confocal timelapse imaging were acquired using Leica LAS-X (version 3.5.7.23225 64-bit). Light-sheet images were acquired using Zen Black (version 3.1) for lightsheet 7 (version 9.3). For X-ray data acquisition see separate Structure Validation report.
Data analysis	Data analysis: Image analysis was performed in ImageJ/Fiji using macros described in Nature Protocols (2020), 15, 450-478 and published on GitHub. Light-sheet images were analysed in Zen Blue (version 3.3) and FIJI. ImageJ v1.52p-1.53t with Java 1.8.0_101-1.8.0_305 were used or FIJI version 2.0.0-rc-69/69/1.52p - 2.9.0/1.53t on MacOS Mojave 10.14.5-Monterey 12.6 was used. PHASER v??? and REFMAC v??? was used for Xray structure analysis.

For manuscripts utilizing custom algorithms or software that are central to the research but not yet described in published literature, software must be made available to editors and reviewers. We strongly encourage code deposition in a community repository (e.g. GitHub). See the Nature Research guidelines for submitting code & software for further information.

Data

Policy information about availability of data

All manuscripts must include a data availability statement. This statement should provide the following information, where applicable:

- Accession codes, unique identifiers, or web links for publicly available datasets
- A list of figures that have associated raw data
- A description of any restrictions on data availability

The data supporting this study are available within the article and the Supplementary Information including the digital data underlying the figures. Other (raw) data supporting this study will be available from the corresponding author upon reasonable request. Plasmids constructed in this study, their maps, and sequences were deposited to the non-profit organization Addgene ID: 189752-189779. The mScarlet3 crystal structure was deposited at the Protein Data Bank as PDB ID: 7ZCT.

Field-specific reporting

Please select the one below that is the best fit for your research. If you are not sure, read the appropriate sections before making your selection.

☒ Life sciences ☐ Behavioural & social sciences ☐ Ecological, evolutionary & environmental sciences

For a reference copy of the document with all sections, see nature.com/documents/nr-reporting-summary-flat.pdf

Life sciences study design

All studies must disclose on these points even when the disclosure is negative.

Sample size	Standard N>3 independent experiments were performed. Number of data, number analyzed cells, and/or technical replicates are indicated in the legends and method section. Sample sizes were not statistically chosen, but estimated empirically from the variation observed in repeated experiments.
Data exclusions	No data is excluded
Replication	Usually three independent replications of the experiments were performed in different transfections on different days. All replications were successful
Randomization	All samples were treated identically (no special additions or stimuli were given).
Blinding	Ratio's, lifetimes, bleaching, phototochromicity, maturation, OSER structures were analyzed blindly using multiwell plates of which both acquisition and analysis was done before confirming the identity of the RFP variant involved. For other experiments no groups were present, for which there was no need for blinding.

Reporting for specific materials, systems and methods

We require information from authors about some types of materials, experimental systems and methods used in many studies. Here, indicate whether each material, system or method listed is relevant to your study. If you are not sure if a list item applies to your research, read the appropriate section before selecting a response.

Materials & experimental systems

n/a	Involved in the study
☒	☐ Antibodies
☐	☒ Eukaryotic cell lines
☒	☐ Palaeontology and archaeology
☐	☒ Animals and other organisms
☒	☐ Human research participants
☒	☐ Clinical data
☒	☐ Dual use research of concern

Methods

n/a	Involved in the study
☒	☐ ChIP-seq
☒	☐ Flow cytometry
☒	☐ MRI-based neuroimaging

Eukaryotic cell lines

Policy information about cell lines

Cell line source(s)	We used U2OS cells (HTB-96, ATCC) or HeLa cells (CCL-2, ATCC).
Authentication	Cell lines were not additionally authenticated

Mycoplasma contamination	Cell lines are routinely checked for Mycoplasma contamination, of which all tests were negative.
Commonly misidentified lines (See ICLAC register)	No commonly misidentified cell lines were used

Animals and other organisms

Policy information about studies involving animals; ARRIVE guidelines recommended for reporting animal research

Laboratory animals	The study did not involve laboratory animals
Wild animals	The study did not involve wild animals
Field-collected samples	The study did not involve samples collected from the field
Ethics oversight	No ethical approval or guidance was required. The regulatory framework on laboratory animals in the European Union does not apply to zebrafish (Danio rerio) larvae that are not yet in their independently feeding larval forms (EU Directive 2010/63, Article 1.3.a.i). The consensus is that zebrafish are in their independently feeding larval forms from 120 hours post-fertilization (hpf) and onwards (10.1016/j.reprotox.2011.06.121.). The zebrafish larvae used in this study did not exceed this threshold.

Note that full information on the approval of the study protocol must also be provided in the manuscript.